# Inelastic collisions of fast charged particles with atoms: Bethe asymptotic formulas and shell corrections

Francesc Salvat [*]
*Facultat de Física (FQA and ICC), Universitat de Barcelona, Diagonal 645, 08028 Barcelona, Spain*

Laia Barjuan
*Facultat de Física (FQA), Universitat de Barcelona, Diagonal 645, 08028 Barcelona, Spain*

Pedro Andreo
*Department of Medical Radiation Physics and Nuclear Medicine, Karolinska University Hospital, SE-17176 Stockholm, Sweden*

(Received 6 November 2021; accepted 25 March 2022; published 20 April 2022)

The relativistic plane-wave Born approximation is applied to the study of inelastic collisions of charged particles with atoms, by considering atomic wave functions calculated from the independent-electron approximation with the self-consistent Dirac-Hartree-Fock-Slater potential. A database of longitudinal and transverse generalized oscillator strengths (GOSs) has been computed by using accurate numerical methods for all the subshells of the ground-state configurations of the elements with atomic numbers from 1 (hydrogen) to 99 (einsteinium). The calculated GOS do not satisfy the Bethe sum rule; departures from the sum rule are in accordance with previous theoretical estimates. Asymptotic high-energy formulas for the total cross section, the stopping cross section, and the energy-straggling cross section are derived with proper account of the relativistic departure from the Bethe sum rule. The shell correction is calculated as the energy-dependent term that, when added to the asymptotic formula, reproduces the value of the atomic cross section calculated by integrating the energy-loss differential cross section. Shell corrections to the stopping cross section obtained from the present approach are presented and compared with previous estimates.

DOI: 10.1103/PhysRevA.105.042813

## I. INTRODUCTION

The slowing down of fast charged particles in matter is primarily due to inelastic collisions, i.e., interactions that involve electronic excitations of the material. The quantum theory of inelastic collisions was formulated by Bethe [1,2] on the basis of the relativistic plane-wave Born approximation (PWBA). The main results of the Bethe theory were reviewed by Inokuti [3] and collaborators [4]. Fano [5] reformulated the relativistic theory by expressing the electromagnetic interaction in the Coulomb gauge, which allows separating the contributions of longitudinal interactions (through the instantaneous Coulomb potential) and transverse interactions (exchange of virtual photons), and by introducing the recoil energy $Q$, defined as the kinetic energy of a free electron with momentum equal to the momentum transfer. Fano's formulation leads to a closed-form expression for the doubly differential cross section (DDCS) for inelastic collisions, differential in the energy transfer, $W$, and the recoil energy, $Q$. Integration of the DDCS over recoil energies gives the energy-loss differential cross section (DCS); the moments of order 0, 1, and 2 of the energy-loss DCS are, respectively, the atomic total cross section, the stopping cross section, and the energy-straggling cross section. Fundamental results from the Bethe theory are the asymptotic (high-energy) formulas for these integrated cross sections.

Bote and Salvat [6] wrote a computer program to calculate ionization cross sections of inner subshells of neutral atoms by impact of electrons and positrons using Fano's formulation of the PWBA. The states of the target atom are described as single Slater determinants built with central-field orbitals that are solutions of the Dirac equation with the self-consistent Dirac-Hartree-Fock-Slater (DHFS) potential of the ground-state configuration [7]. Since the interaction of the projectile and the atomic electrons is considered as a perturbation to first order, the transition matrix elements reduce to sums of one-electron integrals, in accordance with the intuitive picture known as the one-active-electron approximation. The resulting DDCS is expressed in terms of the longitudinal generalized oscillator strength (GOS), which summarizes the response of the target atom to the instantaneous Coulomb interaction, and a transverse generalized oscillator strength (TGOS), which accounts for transverse interactions.

Starting from the program of Bote and Salvat [6], we have developed and assembled a set of computer programs that perform the complete sequence of calculations leading to the energy-loss DCS, the integrated cross sections and the shell corrections. We have run these programs for the subshells of the ground-state configurations of all the atoms in the

[*] francesc.salvat@ub.edu

periodic system, from hydrogen (atomic number $Z = 1$) to einsteinium ($Z = 99$). The calculations involved the generation of a database of longitudinal and transverse GOSs for all electron subshells. Since our calculations are based on the Dirac equation, the calculated longitudinal GOSs do not satisfy the Bethe sum rule [8,9], which states that the integral of the longitudinal GOS over $W$ equals the number $Z$ of electrons in the target atom. This sum rule plays a key role in the derivation of the asymptotic formulas for the integrated cross sections [5], notwithstanding the fact that it holds only in the nonrelativistic domain, i.e., for atoms with low atomic numbers. Calculation results show that the relativistic departure decreases with $Q$, and at $Q = 0$ it is negligible for hydrogen and it increases in magnitude with $Z$ to reach a value of about $-2.5\%$ for $Z = 99$.

The goal of the present work is not to compute realistic total cross sections and stopping powers, because the independent-electron model and the DHFS potential are too simplistic to reproduce the details of the actual excitation spectrum of isolated atoms. Indeed, our framework (PWBA with DHFS potential) provides reliable results only for the ionization of inner-electron subshells by impact of high-energy charged particles, mostly because the relevant one-electron wave functions are practically unaffected by the existence of neighbor atoms. Nevertheless, it allows the numerical calculation of theoretical GOSs to very high accuracy (including contributions from excitations to bound levels), from which energy-loss DCSs can be obtained by numerical integration of the DDCS.

We present a derivation of asymptotic formulas for the total cross section, the stopping cross section, and the energy-straggling cross section by using a method similar to the one adopted by Fano [5] with due account of relativistic departures from the Bethe sum rule. We limit our considerations to projectiles heavier than the electron, because the stopping of high-energy electrons and positrons is dominated by the radiative contribution [10]. The asymptotic formulas are valid in the limit of high kinetic energies. Their departures from the exact cross sections, obtained by integrating the energy-loss DCS, are known as shell corrections [5]. Existing calculations of the shell correction to the stopping cross section are based on nonrelativistic calculations with hydrogenic wave functions or Hartree–Slater wave functions (see Ref. [11] and references therein), or on the free-electron gas theory [12]. In the present work, shell corrections are obtained as differences between the numerical integrated cross sections and the corresponding asymptotic formulas.

Since both shell corrections and departures from the Bethe sum rule get the largest contributions from inner-electron subshells, they are expected to be accurately described within our theoretical framework. Motivated by this expectation, we have devised a consistent scheme to evaluate the impact of departures from the Bethe sum rule on the asymptotic formulas, and to calculate a comprehensive database of shell corrections to the integrated (total, stopping, and energy-straggling) cross sections for neutral atoms with $Z = 1$–$99$.

The present paper is structured as follows. After summarizing relevant formulas obtained from the relativistic PWBA, which have been used to calculate the numerical database of GOSs, we consider the deviation from the Bethe sum rule caused by relativistic effects and the calculation of integrated cross sections. Then we derive asymptotic formulas for the total cross section, the stopping cross section, and the energy straggling cross section of closed electron subshells. Asymptotic formulas for atoms are obtained by adding the contributions from the various subshells. Finally, shell corrections are introduced, and we present numerical estimates of the correction to the formula of the stopping cross section for projectile protons and selected elements.

In the following, all electromagnetic quantities are expressed in the Gaussian system of units (see, e.g., Ref. [13]) and the electromagnetic potentials are in the Coulomb gauge. The symbols $e$, $m_e$, $\hbar$, and $c$ denote, respectively, the elementary charge (i.e., the absolute value of the electron charge), the electron mass, the reduced Planck constant, and the speed of light in vacuum. For the sake of brevity, we use the same notation as in Ref. [6].

## II. PLANE-WAVE BORN APPROXIMATION

In our PWBA calculations, atomic electron wave functions are represented as positive-energy Dirac spherical waves [7,14]

$$\psi_{\epsilon\kappa m}(\mathbf{r}) = \frac{1}{r}\begin{pmatrix} P_{\epsilon\kappa}(r)\,\Omega_{\kappa,m}(\hat{\mathbf{r}}) \\ \mathrm{i}Q_{\epsilon\kappa}(r)\,\Omega_{-\kappa,m}(\hat{\mathbf{r}}) \end{pmatrix}, \tag{1}$$

where $\epsilon$ is the electron energy, exclusive of its rest energy, $\kappa = (\ell - j)(2j + 1)$ is the relativistic angular momentum quantum number, $m$ is the magnetic quantum number, $\Omega_{\kappa,m}(\hat{\mathbf{r}})$ are spherical spinors, and the functions $P_{\epsilon\kappa}(r)$ and $Q_{\epsilon\kappa}(r)$ satisfy the Dirac radial equations with the DHFS self-consistent potential, $V_{\mathrm{DHFS}}(r)$ [7],

$$\begin{aligned} \frac{dP_{\epsilon\kappa}}{dr} &= -\frac{\kappa}{r}P_{\epsilon\kappa} + \frac{\epsilon - V_{\mathrm{DHFS}}(r) + 2m_e c^2}{\hbar c}Q_{\epsilon\kappa}, \\ \frac{dQ_{\epsilon\kappa}}{dr} &= -\frac{\epsilon - V_{\mathrm{DHFS}}(r)}{\hbar c}P_{\epsilon\kappa} + \frac{\kappa}{r}Q_{\epsilon\kappa}. \end{aligned} \tag{2}$$

Bound-state wave functions, with discrete negative energies and normalized to unity, are designated as $\psi_{n\kappa m}$, with the principal quantum number $n$ instead of $\epsilon$. Free states, with positive energy $\epsilon$ are normalized so that the radial function $P(r)$ at large radii oscillates with unit amplitude. Notice that $\kappa$ works as a shorthand for both $j = |\kappa| - 1/2$ and $\ell = j + \kappa/(2|\kappa|)$; the symbol $\overline{\ell}$ designates the value of $\ell$ corresponding to $-\kappa$. States of the projectile are described as Dirac plane waves with positive energy, i.e., the PWBA disregards the distortion of the projectile wave caused by the Coulomb field of the atom. As a consequence, the PWBA is reliable only for projectiles with velocities much larger than the velocities of the electrons in the target atom (see, e.g., Ref. [3]).

We consider inelastic collisions of a charged projectile (charge $Z_0 e$ and mass $M$) with a neutral target atom of the element with atomic number $Z$. Let $E$, $\mathbf{p}$ denote, respectively, the kinetic energy and the momentum of the projectile before the collision,

$$cp = \sqrt{E(E + 2Mc^2)}, \tag{3}$$

and let $E'$, $\mathbf{p}'$ be the corresponding quantities after the interaction,

$$E' = E - W, \quad cp' = \sqrt{(E-W)(E-W+2Mc^2)}, \tag{4}$$

where $W$ is the energy loss. We recall that the kinetic energy and momentum of the projectile can be expressed as

$$E = (\gamma - 1)Mc^2, \quad p = \beta\gamma\, Mc, \tag{5}$$

where

$$\beta = \frac{v}{c} = \sqrt{\frac{\gamma^2-1}{\gamma^2}} = \sqrt{\frac{E(E+2Mc^2)}{(E+Mc^2)^2}} \tag{6}$$

is the speed $v$ in units of $c$, and

$$\gamma = \sqrt{\frac{1}{1-\beta^2}} = \frac{E+Mc^2}{Mc^2} \tag{7}$$

is the total energy of the projectile in units of its rest energy.

Assuming that the target atom is spherically symmetric or randomly oriented, the DDCS is a function of only the energy loss $W$ and the polar scattering angle $\theta$. Following Fano [5], instead of $\theta$, we express the DDCSs in terms of the recoil energy $Q$ defined by

$$Q(Q+2m_ec^2) = (c\hbar q)^2, \tag{8}$$

where $\hbar\mathbf{q} = \mathbf{p} - \mathbf{p}'$ is the momentum transfer. Equivalently,

$$Q = \left[(cp)^2 + (cp')^2 - 2\,cp\,cp'\,\cos\theta + m_e^2c^4\right]^{1/2} - m_ec^2. \tag{9}$$

For a given energy loss, the kinematically allowed recoil energies lie in the interval $Q_- < Q < Q_+$, with endpoints,

$$Q_\pm = \sqrt{[cp \pm cp']^2 + m_e^2c^4} - m_ec^2. \tag{10}$$

For projectiles with high energy and $W \ll E$,

$$Q_-(Q_- + 2m_ec^2) \simeq W^2/\beta^2. \tag{11}$$

From Eq. (10), it is clear that the curves $Q = Q_-(W)$ and $Q = Q_+(W)$ intersect at $W = E$ ($p' = 0$). Thus, they define a single continuous function $W = W_\mathrm{m}(Q)$ in the interval $0 < Q < Q_+(0)$, see Fig. 1. By solving the equations $Q = Q_\pm(W_\mathrm{m})$ we obtain

$$W_\mathrm{m}(Q) = E + Mc^2 - \sqrt{\left[cp - \sqrt{Q(Q+2m_ec^2)}\right]^2 + M^2c^4}, \tag{12}$$

which, when $W \ll E$, reduces to

$$W_\mathrm{m}(Q) \simeq \beta\sqrt{Q(Q+2m_ec^2)}. \tag{13}$$

It follows that, for given values of $E$ and $Q$ [$< Q_+(0)$], the only kinematically allowed values of the energy loss are those in the interval $0 < W < W_\mathrm{m}(Q)$.

Because we are interested in accounting for departures from the Bethe sum rule, we consider the DDCS for transitions of atomic electrons to both bound levels $\epsilon_{n_b\kappa_b}$ (excitation) and free levels $\epsilon_b$ (ionization). The derivation of the final formulas is parallel to the one given in Ref. [6] for ionization, where details of the numerical techniques adopted in the calculations can also be found.

The DDCS for excitations of electrons in the closed subshell $a = (n_a\kappa_a)$ with $2|\kappa_a| = 2j_a + 1$ electrons and ionization energy $E_a = -\epsilon_{n_a\kappa_a}$, splits into contributions from longitudinal and transverse interactions,

$$\frac{d^2\sigma_a}{dW\,dQ} = \frac{d^2\sigma_a^\mathrm{L}}{dW\,dQ} + \frac{d^2\sigma_a^\mathrm{T}}{dW\,dQ}, \tag{14}$$

with (see Eq. (38) in Ref. [6])

$$\frac{d^2\sigma_a^\mathrm{L}}{dW\,dQ} = \mathcal{B}\,\frac{2m_ec^2}{WQ(Q+2m_ec^2)}\,A_\mathrm{L}\,\frac{df_a(Q,W)}{dW} \tag{15}$$

and

$$\frac{d^2\sigma_a^\mathrm{T}}{dW\,dQ} = \mathcal{B}\,\frac{2m_ec^2W}{[Q(Q+2m_ec^2) - W^2]^2} \times A_\mathrm{T}\,\frac{dg_a(Q,W)}{dW}, \tag{16}$$

where

$$\mathcal{B} = \frac{2\pi Z_0^2e^4}{m_ev^2}, \tag{17}$$

$$A_\mathrm{L} = 1 - \frac{4(E+Mc^2)W - W^2 + Q(Q+2m_ec^2)}{4\,(E+Mc^2)^2} \tag{18}$$

and

$$A_\mathrm{T} = \beta^2 - \frac{W^2}{Q(Q+2m_ec^2)}\left(1 + \frac{Q(Q+2m_ec^2) - W^2}{2W(E+Mc^2)}\right)^2 + \frac{Q(Q+2m_ec^2) - W^2}{2(E+Mc^2)^2}. \tag{19}$$

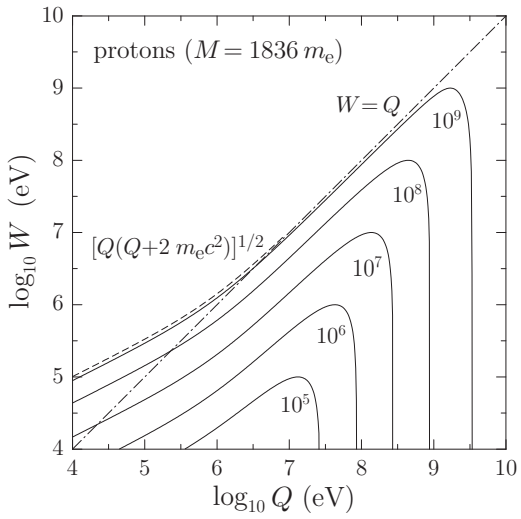


FIG. 1. Domains of kinematically allowed transitions in the $(Q, W)$ plane for protons. The curves represent the maximum allowed energy loss $W_\mathrm{m}(Q)$, given by Eq. (12), for projectiles with the indicated kinetic energies (in eV). When $E$ increases, $W_\mathrm{m}(Q)$ approaches the vacuum photon line, $W_0(Q) = [Q(Q+2m_ec^2)]^{1/2}$ [Eq. (41)], which is an absolute upper bound for the allowed energy losses.

The last factors in Eqs. (15) and (16) are, respectively, the longitudinal and transverse generalized oscillator strengths (GOSs). The longitudinal GOS is given by

$$\frac{df_a(Q,W)}{dW} = \frac{W}{Q}\,\frac{2(Q+m_ec^2)}{Q+2m_ec^2}\sum_{n_b,\kappa_b}\frac{2|\kappa_b|-q_b}{2|\kappa_b|}\,\delta(W-\epsilon_{n_b\kappa_b}+\epsilon_{n_a\kappa_a})$$
$$\times\sum_{\lambda}(2\lambda+1)\left\langle \ell_b\tfrac{1}{2}\,j_b\middle\|\mathbf{C}^{(\lambda)}\middle\|\ell_a\tfrac{1}{2}\,j_a\right\rangle^2\left[R^{\lambda}_{n_b\kappa_b;n_a\kappa_a}(q)\right]^2$$
$$+\frac{W}{Q}\,\frac{2(Q+m_ec^2)}{Q+2m_ec^2}\,\frac{k_b}{\epsilon_b\pi}\sum_{\kappa_b}\sum_{\lambda}(2\lambda+1)\left\langle \ell_b\tfrac{1}{2}\,j_b\middle\|\mathbf{C}^{(\lambda)}\middle\|\ell_a\tfrac{1}{2}\,j_a\right\rangle^2\left[R^{\lambda}_{\epsilon_b\kappa_b;n_a\kappa_a}(q)\right]^2 \tag{20}$$

with the radial integrals

$$R^{\lambda}_{\epsilon_b\kappa_b;n_a\kappa_a}(q)=\int_0^{\infty}\left[P_{\epsilon_b\kappa_b}(r)P_{n_a\kappa_a}(r)+Q_{\epsilon_b\kappa_b}(r)Q_{n_a\kappa_a}(r)\right]j_{\lambda}(qr)\,dr, \tag{21}$$

where $j_\ell(x)$ are the spherical Bessel functions. The two terms on the right-hand side of Eq. (20) are contributions from excitations to bound levels and ionizations, respectively. The quantity $q_b$ is the number of atomic electrons in the excited level $\epsilon_{n_b\kappa_b}$, and the factor $1-q_b/(2|\kappa_b|)$ accounts for the Pauli exclusion principle, which forbids transitions to occupied orbitals. $k_b$ is the electron wave number corresponding to the kinetic energy $\epsilon_b$ of the final free orbital.

The transverse GOS (TGOS) can be expressed as

$$\frac{dg_a(Q,W)}{dW} = \frac{2(Q+m_ec^2)}{W}\sum_{n_b,\kappa_b}\frac{2|\kappa_b|-q_b}{2|\kappa_b|}\,\delta\big(W-\epsilon_{n_b\kappa_b}+\epsilon_{n_a\kappa_a}\big)$$
$$\times\sum_{J}\frac{2J+1}{2J(J+1)}\Big\{\left\langle \ell_b\tfrac{1}{2}\,j_b\middle\|\mathbf{C}^{(J)}\middle\|\ell_a\tfrac{1}{2}\,j_a\right\rangle^2\left[{}^{\mathrm{e}}\mathcal{R}^{J}_{n_b\kappa_b;n_a\kappa_a}(q)\right]^2+\left\langle \ell_b\tfrac{1}{2}\,j_b\middle\|\mathbf{C}^{(J)}\middle\|\overline{\ell}_a\tfrac{1}{2}\,j_a\right\rangle^2\left[{}^{\mathrm{m}}\mathcal{R}^{J}_{n_b\kappa_b;n_a\kappa_a}(q)\right]^2\Big\}$$
$$+\frac{2(Q+m_ec^2)}{W}\,\frac{k_b}{\epsilon_b\pi}\sum_{\kappa_b}\sum_{J}\frac{2J+1}{2J(J+1)}\Big\{\left\langle \ell_b\tfrac{1}{2}\,j_b\middle\|\mathbf{C}^{(J)}\middle\|\ell_a\tfrac{1}{2}\,j_a\right\rangle^2\left[{}^{\mathrm{e}}\mathcal{R}^{J}_{\epsilon_b\kappa_b;n_a\kappa_a}(q)\right]^2$$
$$+\left\langle \ell_b\tfrac{1}{2}\,j_b\middle\|\mathbf{C}^{(J)}\middle\|\overline{\ell}_a\tfrac{1}{2}\,j_a\right\rangle^2\left[{}^{\mathrm{m}}\mathcal{R}^{J}_{n_b\kappa_b;n_a\kappa_a}(q)\right]^2\Big\}, \tag{22}$$

with the radial integrals

$${}^{\mathrm{e}}\mathcal{R}^{J}_{\epsilon_b\kappa_b;n_a\kappa_a}(q)=\frac{J(J+1)}{2J+1}\Big[-\frac{\kappa_b-\kappa_a}{J}\left(F^{J-1}_{\epsilon_b\kappa_b;n_a\kappa_a}+G^{J-1}_{\epsilon_b\kappa_b;n_a\kappa_a}\right)+\left(F^{J-1}_{\epsilon_b\kappa_b;n_a\kappa_a}-G^{J-1}_{\epsilon_b\kappa_b;n_a\kappa_a}\right)$$
$$+\frac{\kappa_b-\kappa_a}{J+1}\left(F^{J+1}_{\epsilon_b\kappa_b;n_a\kappa_a}+G^{J+1}_{\epsilon_b\kappa_b;n_a\kappa_a}\right)+\left(F^{J+1}_{\epsilon_b\kappa_b;n_a\kappa_a}-G^{J+1}_{\epsilon_b\kappa_b;n_a\kappa_a}\right)\Big] \tag{23}$$

and

$${}^{\mathrm{m}}\mathcal{R}^{J}_{\epsilon_b\kappa_b;n_a\kappa_a}(q)=(\kappa_a+\kappa_b)\left(F^{J}_{\epsilon_b\kappa_b;n_a\kappa_a}+G^{J}_{\epsilon_b\kappa_b;n_a\kappa_a}\right), \tag{24}$$

where

$$F^{J}_{\epsilon_b\kappa_b;n_a\kappa_a}=\int_0^{\infty}P_{\epsilon_b\kappa_b}(r)\,Q_{n_a\kappa_a}(r)\,j_J(qr)\,dr\quad\text{and}\quad G^{J}_{\epsilon_b\kappa_b;n_a\kappa_a}=\int_0^{\infty}Q_{\epsilon_b\kappa_b}(r)\,P_{n_a\kappa_a}(r)\,j_J(qr)\,dr. \tag{25}$$

The quantities $\langle \ell_b\frac{1}{2}\,j_b||\mathbf{C}^{(L)}||\ell_a\frac{1}{2}\,j_a\rangle$ are the reduced matrix elements of the Racah tensors,[1]

$$\left\langle \ell_b\tfrac{1}{2}\,j_b\middle\|\mathbf{C}^{(L)}\middle\|\ell_a\tfrac{1}{2}\,j_a\right\rangle=\upsilon(L,\ell_b,\ell_a)\,\sqrt{2j_a+1}\,\langle Lj_a0\tfrac{1}{2}|j_b\tfrac{1}{2}\rangle, \tag{26}$$

where

$$\upsilon(L,\ell_b,\ell_a)\equiv\begin{cases}1\text{ if }L+\ell_b+\ell_a\text{ is even}\\0\text{ otherwise,}\end{cases} \tag{27}$$

and $\langle Lj_a0\frac{1}{2}|j_b\frac{1}{2}\rangle$ is a Clebsch-Gordan coefficient. It is worth noticing that in the limit $Q\to 0$ both the longitudinal and transverse GOSs reduce to the optical oscillator strength (OOS),

$$-\frac{df_a(0,W)}{dW}=\frac{dg_a(0,W)}{dW}=\frac{df_a(W)}{dW}. \tag{28}$$

As mentioned in Sec. I, we have generated a numerical database of longitudinal and transverse GOSs for all the subshells of neutral atoms with $Z=1$–99 in their ground-state configuration. For each subshell, the database tables include the GOSs for excitations to discrete levels (occupied and

[1]Equation (52) of Ref. [6] contains a typo.

unoccupied) with principal quantum numbers $n_b$ up to 25 as functions of $Q$, as well as the GOSs for ionization as functions of $W$ and $Q$. The numerical values cover finite intervals of $Q$ and $W$ extending up to certain maximum values, $Q_{\rm num}$ and $W_{\rm num}$, at which the adopted calculation methods are considered to become inaccurate. The numerical solution of the radial Dirac equation [7] is not possible for bound states with $n_b$ larger than about 30, and for free states with $\epsilon_b$ less than about $10^{-4}$ atomic units. The GOS in the narrow $W$ interval corresponding to excitations with $n_b > 25$ and ionizations with $\epsilon_b < 10^{-4}$ hartrees is assumed to be constant and equal to the ionization GOS at the lowest calculable energy loss. Generally, the calculated GOS values are expected to be accurate to five significant digits [6]. To ensure accuracy of the energy-loss DCS and its integrals, specific schemes are adopted for interpolating and extrapolating the numerical GOS tables [6].

The calculated GOSs and TGOSs for ionization of the $M1$ ($3s_{1/2}$) subshell of silver ($Z = 47$) are displayed in Fig. 2. The representation of the GOS for ionization as a surface on the $(Q, W)$ plane is called the Bethe surface [3]. As illustrated in Fig. 2, for energy losses $W$ larger than about $2E_a$, the GOS has a prominent maximum at $W \sim Q$), the Bethe ridge [3], which corresponds to collisions with relatively large momentum transfers (close collisions). The TGOS can be represented in a similar way; its Bethe surface is analogous to that of the GOS, one differentiating feature being that beyond the Bethe ridge, i.e., for $Q > W$, the TGOS decreases more slowly than the GOS.

### A. Bethe sum

In the nonrelativistic theory the subshell (longitudinal) GOS satisfies the Bethe sum rule [3,5]

$$\int_0^\infty \frac{df_a(Q,W)}{dW}\,dW = 2|\kappa_a| \qquad \forall Q, \tag{29}$$

where the integral extends over all possible one-electron transitions. In addition, the subshell GOS is assumed to be calculated by assuming that all bound orbitals are empty, i.e., by setting $q_b = 0$ and, consequently, disregarding restrictions imposed by the exclusion principle. Notice that the contribution to the GOS of transitions to levels with energies higher (lower) than the initial level are positive (negative). When adding the contributions of the subshells to get the atomic GOS (see below), contributions of up and down transitions between occupied bound levels cancel each other and, as a result, there is a net transfer of GOS from inner to outer subshells.

Theoretical studies [8,9,15] show that relativistic effects cause deviations from the Bethe sum rule at small and moderate $Q$. The relativistic generalization of the integral (29) is the Bethe sum

$$S_0(a;Q) \equiv \int_0^\infty \frac{df_a(Q,W)}{dW}\,dW. \tag{30}$$

The functions $S_0(a;Q)$ for the subshells of gold ($Z = 79$) atoms, calculated from the numerical GOS tables, are displayed in Fig. 3 as functions of the reduced recoil energy $Q/E_a$, where $E_a = -\epsilon_{n_a\kappa_a}$ is the ionization energy of the

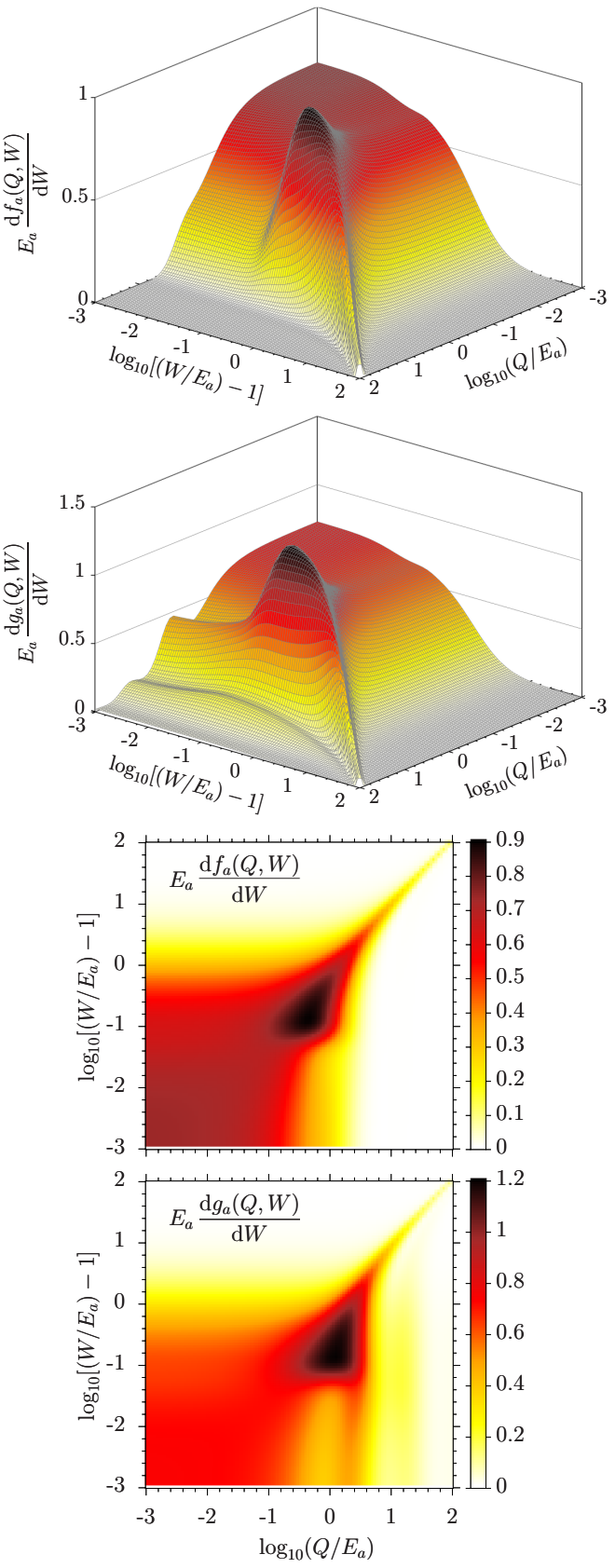


FIG. 2. The GOS and the TGOS for ionization of the $M1$ subshell ($3s_{1/2}$) of the silver atom ($Z = 47$), represented as Bethe three-dimensional surfaces (top) and as color-level diagrams (bottom).

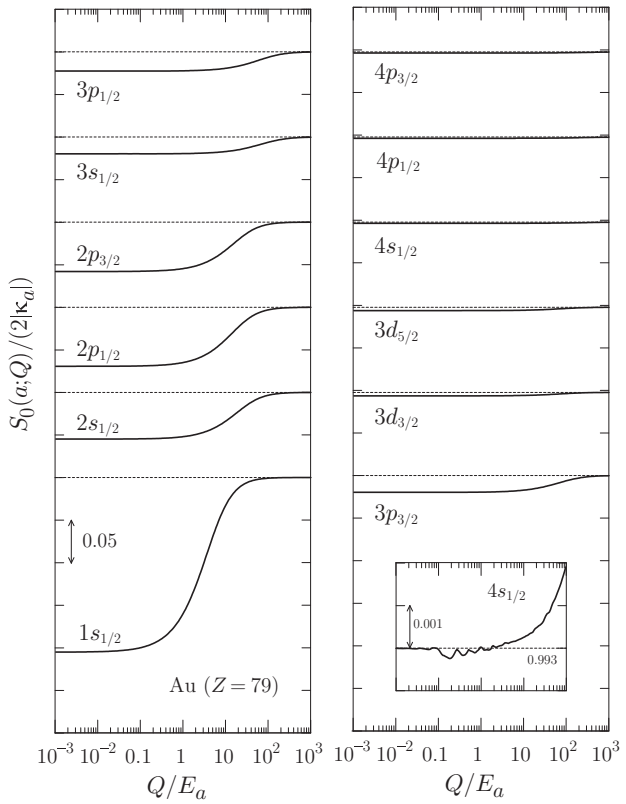


FIG. 3. Normalized sum $S_0(a;Q)/(2|\kappa_a|)$ for various subshells of gold atoms ($Z = 79$), as functions of the reduced recoil energy $Q/E_a$. Each curve is plotted with its own vertical axis, which is shifted an arbitrary number of divisions to accommodate several subshells in the same plot, and all curves are drawn with the same scale. The division length of the vertical axis is indicated in the plot. The dashed horizontal lines represent the asymptotic value of each curve, which equals unity. The inset shows the sum for the $4s_{1/2}$ subshell in an expanded scale, to reveal the magnitude of accumulated numerical errors.

active subshell. The relativistic departure $\Delta(a;Q) = 1 - S_0(a;Q)/(2|\kappa_a|)$ decreases with $Q$; its value at $Q = 0$ is larger for the $K$ ($1s_{1/2}$) shell and decreases when the principal quantum number $n_a$ increases, i.e., when the ionization energy decreases.

To check the global accuracy of our calculated $S_0(a;Q)$ values, we have performed calculations of the Bethe sum from nonrelativistic GOSs obtained by running our code with the speed of light $c$ replaced with a value 1000 times larger; the resulting sum was found to agree with the number of electrons for recoil energies up to the largest value attainable, $Q_{\rm num}$, the relative differences being less than $\sim 10^{-4}$ in all cases.

For energy transfers $W$ much larger than the ionization energy $E_a$ of the active subshell, atomic electrons respond as if they were free and at rest. Under these circumstances, the finite width of the Bethe ridge can be neglected (see Fig. 2), i.e., the GOSs can be approximated as

$$\frac{df_a(Q,W)}{dW} = \frac{dg_a(Q,W)}{dW} = 2|\kappa_a|\,\delta(W-Q). \tag{31}$$

### B. Atomic cross sections

The DDCS for inelastic collisions with an atom is obtained by adding the contributions of the different electron subshells. That is, the atomic DDCS takes the same form as the DDCS of individual subshells, Eqs. (14)–(19), with the subshell GOSs $df_a(Q,W)/dW$ and $dg_a(Q,W)/dW$ replaced with the atomic GOSs given by

$$\frac{df(Q,W)}{dW} = \sum_{n_a\kappa_a} \frac{q_a}{2|\kappa_a|}\frac{df_a(Q,W)}{dW} \tag{32}$$

and

$$\frac{dg(Q,W)}{dW} = \sum_{n_a\kappa_a} \frac{q_a}{2|\kappa_a|}\frac{dg_a(Q,W)}{dW}, \tag{33}$$

where the summations run over the occupied subshells of the ground-state configuration. In the case of an open subshell ($n_a\kappa_a$) with $q_a$ electrons ($q_a < 2|\kappa_a|$), its contribution to the atomic GOSs is approximated by the product of the fractional occupancy, $q_a/2|\kappa_a|$, and the GOS of the closed subshell.

The energy-loss DCS (i.e., the DCS as a function of only the energy loss $W$) is obtained by integrating the DDCS over the recoil energy,

$$\frac{d\sigma}{dW} = \int_{Q_-}^{Q_+} \frac{d^2\sigma}{dW\,dQ}\,dQ. \tag{34}$$

Evidently, the energy-loss DCS is defined only for energy losses that are less than $W_{\rm max} = E$.

We consider the integrals (moments) of the energy-loss DCS,

$$\sigma^{(i)} \equiv \int_0^{W_{\rm max}} W^i\,\frac{d\sigma}{dW}\,dW. \tag{35}$$

$\sigma^{(0)}$ is the total inelastic cross section. $\sigma^{(1)}$ and $\sigma^{(2)}$ are known as the stopping cross section and the energy straggling cross section (for inelastic collisions), respectively. Since the probability density of the energy loss $W$ in a single collision is

$$p_1(W) = \frac{1}{\sigma_0}\,\frac{d\sigma}{dW}, \tag{36}$$

we can write

$$\sigma^{(i)} = \sigma^{(0)}\int_0^{W_{\rm max}} W^i\,p_1(W)\,dW = \sigma^{(0)}\,\langle W^i\rangle, \tag{37}$$

where $\langle W^i\rangle$ is the average value of $W^i$ in a single collision.

When the fast projectile is moving in a monoatomic gas of the element of atomic number $Z$ with $\mathcal{N}$ atoms per unit volume, the mean-free path $\lambda$ for inelastic collisions is given by

$$\lambda = 1/(\mathcal{N}\sigma^{(0)}). \tag{38}$$

Its inverse, $\lambda^{-1} = \mathcal{N}\sigma^{(0)}$, is the probability of collision per unit path length. The (collision) stopping power $S$ and the energy straggling parameter $\Omega^2$ are defined by

$$S = \mathcal{N}\sigma^{(1)} = \frac{\langle W\rangle}{\lambda} \tag{39}$$

and

$$\Omega^2 = \mathcal{N}\sigma^{(2)} = \frac{\langle W^2\rangle}{\lambda}, \tag{40}$$

respectively. Evidently, the stopping power gives the average energy loss per unit path length. The product $\Omega^2\, ds$ is the variance of the energy distribution of an originally monoenergetic beam after a short path length $ds$ (see, e.g., Ref. [16]).

Values of the integrated cross sections $\sigma^{(0)}$, $\sigma^{(1)}$, and $\sigma^{(2)}$ for collisions of protons with atoms have been calculated for all the elements from $Z = 1$–99. The calculations were made for a grid of kinetic energies that extended from 1 keV to 100 GeV, with nearly logarithmic spacing and 20 points per decade. Comparison of the results with the asymptotic formulas derived below (and evaluated by using alternative numerical methods) indicates that the numerical errors accumulated throughout the lengthy calculation of integrated cross sections are less than about 0.5% for energies up to 10 GeV.

## III. BETHE ASYMPTOTIC FORMULAS

Bethe [1,2] (see also Refs. [5] and [3]) derived simple and accurate analytical formulas for the stopping cross section and the total cross section for high-energy projectiles, which are among the most useful formulas in radiation physics. Their usefulness stems from the fact that each formula contains only two parameters, which are characteristic of each element or material. These parameters can be inferred from experimental measurements of the stopping power and the total cross section. Thus, the Bethe formulas with empirically determined parameters provide reliable values of these cross sections for different kinds of charged particles, and in a wide energy range, for molecules and condensed materials for which first-principles calculations are not available or possible. Although the Bethe formulas are asymptotic (i.e., valid only for projectiles with very high energies), they remain fairly accurate down to moderately low energies (see below).

In the present section, we derive asymptotic formulas for $\sigma^{(i)}$ ($i = 0$, 1, and 2) by using a method similar to the one adopted in Fano's [5] review. The conventional derivation of the stopping power formula makes explicit use of the Bethe sum rule, Eq. (29), which is correct only for sufficiently large recoil energies. In our derivation we allow deviations from that sum rule for small and intermediate recoil energies.

For the sake of simplicity, we shall derive first asymptotic formulas for excitations of a single closed electron subshell $a = (n_a\kappa_a)$ with ionization energy $E_a$. We start from the DDCS given by Eqs. (14)–(19). For high-energy projectiles, the relevant energy transfers are such that $W \ll E$ and the minimum allowed recoil energy $Q_-$ is given by Eq. (11),

$$Q_-(Q_- + 2m_ec^2) = W^2/\beta^2,$$

where we have disregarded terms containing factors $W/E$. Within the same approximation, and for small and moderate recoil energies, the maximum allowed energy loss is [Eq. (13)]

$$W_{\rm m}(Q) = \beta\sqrt{Q(Q + 2m_ec^2)}.$$

When the energy of the projectile increases, both $Q_-(W)$ and $W_{\rm m}(Q)$ tend towards the vacuum photon line,

$$W_0(Q) = \sqrt{Q(Q + 2m_ec^2)}. \tag{41}$$

The recoil energy at this line is

$$Q_0(W) = m_ec^2\left[\sqrt{1 + \left(\frac{W}{m_ec^2}\right)^2} - 1\right] \simeq \frac{W^2}{2m_ec^2}\left[1 - \left(\frac{W}{2m_ec^2}\right)^2 + \cdots\right]. \tag{42}$$

That is, recoil energies less than $Q_0(W)$ and energy losses larger than $W_0(Q)$ are not attainable in inelastic collisions. For the most probable excitations, $W$ is much less than $2m_ec^2$ and $Q_0(W)$ is closely approximated by the first term of the expansion (42), i.e., $Q_0(W) \simeq W^2/2m_ec^2$.

Following Fano [5], we evaluate the integrals of the DDCS (14) approximately by considering various ranges of $Q$. For recoil energies smaller than about $0.01\,W$, the GOS and the TGOS practically coincide with the OOS. Hence, we may introduce a cutoff recoil energy $Q_1 \simeq 0.001\,E_a$, and consider that for $Q < Q_1$ both the GOS and the TGOS are approximately equal to the OOS, $df_a(W)/dW$ (dipole approximation). For recoil energies between $Q_1$ and a certain value $Q_2$, which we assume much larger than the ionization energy of the atomic electrons, the maximum allowed energy transfer $W_{\rm m}(Q)$ is sufficiently large to include the practical totality of the GOS, i.e., to exhaust the Bethe sum. In our calculations we set $Q_2 = \max(10^4E_a, 10^5E_{\rm h})$, where $E_{\rm h}$ is the Hartree energy. We have verified that for recoil energies higher than $Q_2$ the GOSs reduce to the Bethe ridge and the Bethe sum rule (29) is satisfied, i.e., the subshell DDCS can be approximated by that of binary collisions with $q_a$ free electrons at rest.

Although an impact parameter is not defined in the PWBA, the classical picture suggests that large (small) momentum transfers roughly correspond to small (large) impact parameters. In fact, interactions with small and large recoil energies are frequently referred to as distant and close interactions, respectively.

### A. Interactions with small and intermediate $Q$

The contribution of distant interactions, with $Q < Q_2$, to the energy-loss DCS can be estimated by assuming that $Q_2 \ll 2m_ec^2$. Then, for energy losses much smaller than $E$ we have,

$$Q_- = W^2/(2m_ec^2\beta^2), \tag{43}$$

The DDCS for longitudinal distant interactions, Eq. (15), can be approximated as

$$\frac{d^2\sigma_a^{\rm L,d}}{dW\,dQ} \simeq \mathcal{B}\,\frac{1}{WQ}\,\frac{df_a(Q,W)}{dW}\,\Theta(Q_2 - Q), \tag{44}$$

where we have neglected terms proportional to $(E + Mc^2)^{-1}$ (which do not contribute in the asymptotic limit) and we have inserted the Heaviside unit step function $\Theta(x)$ (= 1 if $x > 0$ and = 0 otherwise), to indicate that this DDCS vanishes if $Q > Q_2$. The corresponding energy-loss DCS is

$$\frac{d\sigma_a^{\rm L,d}}{dW} = \int_{Q_-}^{Q_2} dQ\,\frac{d^2\sigma_a^{\rm L,d}}{dW\,dQ} = \mathcal{B}\,\frac{1}{W}\int_{Q_-}^{Q_2}\frac{dQ}{Q}\,\frac{df_a(Q,W)}{dW}\,\Theta(Q_2 - Q). \tag{45}$$

It is convenient to remove the energy dependence of the lower limit of this integral by writing

$$\frac{d\sigma_a^{\mathrm{L,d}}}{dW} = \mathcal{B}\,\frac{1}{W}\left(\int_{Q_0}^{Q_2}\frac{dQ}{Q}\,\frac{df_a(Q,W)}{dW} - \int_{Q_0}^{Q_-}\frac{dQ}{Q}\,\frac{df_a(Q,W)}{dW}\right)\Theta(Q_2-Q), \quad (46)$$

where $Q_0$ is the recoil energy of the vacuum photon line, Eq. (42). If the kinetic energy of the projectile is high enough, the second integral in (46) involves only small recoil energies, for which the dipole approximation is applicable, and

$$\int_{Q_0}^{Q_-}\frac{dQ}{Q}\,\frac{df_a(Q,W)}{dW} \simeq \frac{df_a(W)}{dW}\int_{Q_0}^{Q_-}\frac{dQ}{Q} = \frac{df_a(W)}{dW}\ln\left(\frac{Q_-}{Q_0}\right) \simeq -\frac{df_a(W)}{dW}\ln\beta^2, \quad (47)$$

where we have used the approximations

$$Q_- \simeq W^2/(2m_\mathrm{e}c^2\beta^2) \quad \text{and} \quad Q_0 \simeq W^2/(2m_\mathrm{e}c^2). \quad (48)$$

Notice that the latter is valid only for energy losses such that $W \ll 2m_\mathrm{e}c^2$ and, therefore, the following formulas have limited accuracy for the innermost subshells of heavy elements, whose $K$ shells have binding energies $E_a$ of the order of 100 keV ($\sim 0.2 m_\mathrm{e}c^2$). Now we can write

$$\frac{d\sigma_a^{\mathrm{L,d}}}{dW} = \mathcal{B}\,\frac{1}{W}\left(\int_{Q_0}^{Q_2}\frac{dQ}{Q}\,\frac{df_a(Q,W)}{dW} + \frac{df_a(W)}{dW}\ln\beta^2\right)\Theta(Q_2-Q). \quad (49)$$

The DDCS of transverse distant interactions is obtained from Eq. (16) after removing terms proportional to $(E + Mc^2)^{-1}$,

$$\frac{d^2\sigma_a^{\mathrm{T,d}}}{dW\,dQ} = \mathcal{B}\,\frac{2m_\mathrm{e}c^2W}{[Q(Q+2m_\mathrm{e}c^2)-W^2]^2} \times\left(\beta^2 - \frac{W^2}{Q(Q+2m_\mathrm{e}c^2)}\right)\frac{dg_a(Q,W)}{dW}\,\Theta(Q_2-Q). \quad (50)$$

The contribution of these excitations to the energy-loss DCS is

$$\frac{d\sigma_a^{\mathrm{T,d}}}{dW} = \int_{Q_-}^{Q_2} dQ\,\frac{d^2\sigma_a^{\mathrm{T,d}}}{dW\,dQ} = \mathcal{B}\int_{Q_-}^{Q_2} dQ\,\frac{2m_\mathrm{e}c^2W}{[Q(Q+2m_\mathrm{e}c^2)-W^2]^2} \times\left(\beta^2 - \frac{W^2}{Q(Q+2m_\mathrm{e}c^2)}\right)\frac{dg_a(Q,W)}{dW}\,\Theta(Q_2-Q).$$

Following Fano [5], because the DDCS (50) decreases rapidly with $Q$, we will replace the TGOS with the OOS (dipole approximation). In addition, to allow the analytical evaluation of the integral, we multiply the integrand by a factor $(Q + m_\mathrm{e}c^2)/m_\mathrm{e}c^2$, which approaches unity for small $Q$. This gives

$$\frac{d\sigma_a^{\mathrm{T,d}}}{dW} = \mathcal{B}\,\frac{df_a(W)}{dW}\int_{Q_-}^{Q_2} dQ\,\frac{2(Q+m_\mathrm{e}c^2)W}{[Q(Q+2m_\mathrm{e}c^2)-W^2]^2} \times\left(\beta^2 - \frac{W^2}{Q(Q+2m_\mathrm{e}c^2)}\right)\Theta(Q_2-Q). \quad (51)$$

To evaluate the integral we introduce the angle $\vartheta_\mathrm{r}$ defined by

$$\cos^2\vartheta_\mathrm{r}(Q) \equiv \frac{W^2/\beta^2}{Q(Q+2m_\mathrm{e}c^2)} \quad (52)$$

and write

$$\frac{d\sigma_a^{\mathrm{T,d}}}{dW} = \mathcal{B}\,\frac{df_a(W)}{dW}\,\frac{1}{W}\int_{Q_-}^{Q_2} dQ \times\left[-\left\{\frac{\beta^4(1-\cos^2\vartheta_\mathrm{r})}{(1-\beta^2\cos^2\vartheta_\mathrm{r})^2}\right\}\frac{d(\cos^2\vartheta_\mathrm{r})}{dQ}\right]. \quad (53)$$

The function in curly brackets equals unity at $\cos^2\vartheta_\mathrm{r} = 0$, which corresponds to large $Q$ values, and vanishes at $\cos^2\vartheta_\mathrm{r}(Q_-) = 1$; this function has a single maximum at $\cos^2\vartheta_\mathrm{r} = 2 - \beta^{-2}$, the width of which decreases when the speed of the particle increases. At high energies, the sharpness of this maximum makes the numerical calculation of the integral of the transverse DDCS over $Q$ difficult. With the dipole approximation the dependence of the GOSs on $Q$ is removed and the integral over $Q$ can be calculated analytically. This gives

$$\frac{d\sigma_a^{\mathrm{T,d}}}{dW} = \mathcal{B}\,\frac{df_a(W)}{dW}\,\frac{1}{W} \times\left[-\frac{\beta^2-1}{1-\beta^2\cos^2\vartheta_\mathrm{r}} + \ln(1-\beta^2\cos^2\vartheta_\mathrm{r})\right]_1^{\cos\vartheta_\mathrm{r}(Q_2)}. \quad (54)$$

When the energy of the projectile is sufficiently high, the most probable distant interactions involve energy transfers that are much less than $W_\mathrm{m}(Q_2)$, for which $Q_- \ll Q_2$ and $\cos^2\vartheta_\mathrm{r}(Q_2) \simeq 0$. To get simpler formulas, we shall set $\cos^2\vartheta_\mathrm{r}(Q_2) = 0$, which amounts to extending the integral over $Q$ values larger than $Q_2$ or, equivalently, to removing the $\Theta(Q_2 - Q)$ function in Eq. (51). Thus, expression (54) simplifies to

$$\frac{d\sigma_a^{\mathrm{T,d}}}{dW} = \mathcal{B}[-\beta^2 - \ln(1-\beta^2)]\frac{1}{W}\,\frac{df_a(W)}{dW}. \quad (55)$$

The energy-loss DCS for distant interactions can now be expressed as

$$\frac{d\sigma_a^{\mathrm{d}}}{dW} = \frac{d\sigma_a^{\mathrm{L,d}}}{dW} + \frac{d\sigma_a^{\mathrm{T,d}}}{dW} \simeq \mathcal{B}\left\{\frac{1}{W}\int_{Q_0}^{Q_2}\frac{dQ}{Q}\,\frac{df_a(Q,W)}{dW} + \frac{1}{W}\,\frac{df_a(W)}{dW}\ln\beta^2 + [-\beta^2 - \ln(1-\beta^2)]\frac{1}{W}\,\frac{df_a(W)}{dW}\right\}. \quad (56)$$

The integrated cross sections for distant interactions are

$$\left[\sigma_a^{\rm d}\right]^{(i)} = \int_0^{W_{\rm m}(Q_2)} W^i \frac{d\sigma_a^{\rm d}}{dW}\, dW.$$

Recalling that that $W_{\rm m}(Q_2)$ is assumed to be sufficiently large to exhaust the Bethe sum, it can be replaced with $\infty$ to give

$$\left[\sigma_a^{\rm d}\right]^{(i)} \simeq \mathcal{B}\left[\ln\left(\frac{\beta^2}{1-\beta^2}\right) - \beta^2\right]\int_0^\infty W^{i-1}\,\frac{df_a(W)}{dW}\,dW + \mathcal{B}\int_0^\infty dW\; W^{i-1}\int_{Q_0}^{Q_2}\frac{dQ}{Q}\,\frac{df_a(Q,W)}{dW}. \tag{57}$$

To evaluate the integrals

$$\mathcal{X}_i \equiv \int_0^\infty dW\; W^{i-1}\int_{Q_0}^{Q_2}\frac{dQ}{Q}\,\frac{df_a(Q,W)}{dW} \tag{58}$$

we first separate the low-$Q$ interval where the dipole approximation is valid ($Q < Q_1$),

$$\begin{aligned}\mathcal{X}_i &\simeq \int_0^\infty dW\; W^{i-1}\int_{Q_0}^{Q_1}\frac{dQ}{Q}\,\frac{df_a(W)}{dW} + \int_0^\infty dW\; W^{i-1}\int_{Q_1}^{Q_2}\frac{dQ}{Q}\,\frac{df_a(Q,W)}{dW}\\ &= \int_0^\infty dW\; W^{i-1}\ln\left(\frac{Q_1}{Q_0}\right)\frac{df_a(W)}{dW} + \int_0^\infty dW\; W^{i-1}\int_{Q_1}^{Q_2}\frac{dQ}{Q}\,\frac{df_a(Q,W)}{dW}.\end{aligned}$$

Exchanging the order of the integrals in the second term, we have

$$\mathcal{X}_i = \int_0^\infty dW\; W^{i-1}\ln\left(\frac{Q_1}{Q_0}\right)\frac{df_a(W)}{dW} + \int_{Q_1}^{Q_2}\frac{dQ}{Q}\,S_{i-1}(a;Q),$$

with

$$S_i(a;Q) \equiv \int_0^\infty W^i\,\frac{df_a(Q,W)}{dW}\,dW. \tag{59}$$

Notice that at sufficiently large $Q$s the GOSs can be approximated as $q_a\delta(W-Q)$ and, consequently, $S_i(a;Q) \sim q_a Q^i$. Introducing the approximation $Q_0 = W^2/(2m_{\rm e}c^2)$ we can write

$$\mathcal{X}_i = S_{i-1}(a)\ln(2m_{\rm e}c^2\,Q_1) - 2S_{i-1}(a)\,\ln[I_{i-1}(a)] + \int_{Q_1}^{Q_2}\frac{dQ}{Q}\,S_{i-1}(a;Q), \tag{60}$$

where

$$S_i(a) \equiv S_i(a;0) = \int_0^\infty W^i\,\frac{df_a(W)}{dW}\,dW \tag{61}$$

and

$$\ln[I_i(a)] = \frac{1}{S_i(a)}\int_0^\infty W^i\,\ln W\,\frac{df_a(W)}{dW}\,dW. \tag{62}$$

With these results, the integrated cross sections for distant interactions, Eq. (57), can be expressed as

$$\left[\sigma_a^{\rm d}\right]^{(i)} \simeq \mathcal{B}\left\{\left[\ln\left(\frac{\beta^2}{1-\beta^2}\right) - \beta^2\right]S_{i-1}(a) + S_{i-1}(a)\ln(2m_{\rm e}c^2\,Q_1) - 2S_{i-1}(a)\,\ln[I_{i-1}(a)] + \int_{Q_1}^{Q_2}\frac{dQ}{Q}\,S_{i-1}(a;Q)\right\}. \tag{63}$$

### B. Close interactions

Close interactions, with $Q > Q_2$, will be described as binary collisions with stationary free electrons. In this case, the largest allowed energy loss is that of the intersection of the curve $W_{\rm m}(Q)$, Eq. (12), with the diagonal $W = Q$, the Bethe ridge, which is given by

$$W_{\rm ridge} = 2\beta^2\gamma^2 m_{\rm e}c^2 R \tag{64}$$

with

$$R = \left[1 + \left(\frac{m_{\rm e}}{M}\right)^2 + 2\gamma\,\frac{m_{\rm e}}{M}\right]^{-1}. \tag{65}$$

Notice that $R \simeq 1$, except for projectiles with mass $M$ comparable to the electron mass. The energy-loss DCS is given by Eq. (14) with the GOSs (31). It can be expressed as

$$\frac{d\sigma_a^{\rm c}}{dW} = \mathcal{B}\,2|\kappa_a|\,\frac{1}{W^2}\,F_{\rm rel}(W)\,\Theta(W-Q_2)\,\Theta(W_{\rm ridge}-W), \tag{66}$$

with

$$F_{\rm rel}(W) = 1 - \beta^2\,\frac{W}{W_{\rm ridge}} + \frac{1-\beta^2}{2M^2c^4}\,W^2. \tag{67}$$

The contributions of close interactions to the integrated cross sections are

$$\begin{aligned}\left[\sigma_a^{\rm c}\right]^{(i)} &= \int_{Q_2}^{W_{\rm ridge}} W^i\,\frac{d\sigma_a^{\rm c}}{dW}\,dW\\ &= \mathcal{B}\,2|\kappa_a|\int_{Q_2}^{W_{\rm ridge}} W^{i-2}\,F_{\rm rel}(W)\,dW.\end{aligned} \tag{68}$$

These integrals can be evaluated analytically. In the high-energy limit ($W_{\rm ridge} \gg Q_2$) they reduce to

$$\left[\sigma_a^{\rm c}\right]^{(0)} \simeq \mathcal{B}\,2|\kappa_a|\,\frac{1}{Q_2}, \tag{69}$$

$$\left[\sigma_a^{\rm c}\right]^{(1)} \simeq \mathcal{B}\,2|\kappa_a|\left[\ln\left(\frac{2m_{\rm e}c^2\beta^2 R}{(1-\beta^2)\,Q_2}\right) - \beta^2 + \left(\frac{m_{\rm e}}{M}\beta^2\gamma R\right)^2\right], \tag{70}$$

$$\left[\sigma_a^{\rm c}\right]^{(2)} \simeq \mathcal{B}\,2|\kappa_a|\left[-Q_2 + (2-\beta^2)\,\frac{m_{\rm e}c^2\,\beta^2}{1-\beta^2}R + \frac{4}{3}\,\frac{m_{\rm e}^2}{M^2}\,\beta^6\gamma^4\,m_{\rm e}c^2R^3\right]. \tag{71}$$

### C. Integrated subshell cross sections

We can now derive asymptotic formulas of the integrated cross sections $\sigma_a^{(i)}$ for excitations of a subshell $n_a\kappa_a$ with $q_a$ ($\leqslant 2|\kappa_a|$) electrons. Hereafter, the subshell GOS and TGOS are

assumed to describe only real transitions that are allowed by Pauli's exclusion principle, that is, transitions to empty final states.

#### 1. Total cross section

The total cross section for distant interactions is given by Eq. (63),

$$\left[\sigma_a^{\rm d}\right]^{(0)} \simeq \mathcal{B}\left\{\left[\ln\left(\frac{\beta^2}{1-\beta^2}\right)-\beta^2\right]S_{-1}(a) + S_{-1}(a)\ln(2m_{\rm e}c^2\,Q_1) - 2S_{-1}(a)\,\ln[I_{-1}(a)] + \int_{Q_1}^{Q_2}\frac{dQ}{Q}\,S_{-1}(a;Q)\right\}, \tag{72}$$

where

$$S_{-1}(a) = \int_0^\infty \frac{1}{W}\,\frac{df_a(W)}{dW}\,dW \tag{73}$$

is the total dipole matrix element squared [3] and

$$\ln[I_{-1}(a)] = \frac{1}{S_{-1}(a)}\int_0^\infty \frac{1}{W}\,\ln W\,\frac{df_a(W)}{dW}\,dW. \tag{74}$$

The total cross section is obtained by adding to this result the contribution from close collisions, given by Eq. (69) with the occupancy $q_a$ of the subshell,

$$\left[\sigma_a^{\rm c}\right]^{(0)} = \mathcal{B}\,q_a\,\frac{1}{Q_2}. \tag{75}$$

We have

$$\sigma_a^{(0)} = \mathcal{B}\left\{S_{-1}(a)\left[\ln\left(\frac{\beta^2}{1-\beta^2}\right)-\beta^2\right] + 2\,S_{-1}(a)\ln\left(\frac{2m_{\rm e}c^2}{I_{-1}(a)}\right)+D_{-1}(a)\right\}, \tag{76}$$

with

$$D_{-1}(a) = S_{-1}(a)\ln\left(\frac{Q_1}{2m_{\rm e}c^2}\right) + \int_{Q_1}^{Q_2}\frac{dQ}{Q}\,S_{-1}(a;Q) + q_a\,\frac{1}{Q_2}. \tag{77}$$

#### 2. Stopping cross section

The stopping cross section for distant interactions, see Eq. (63), can be written as

$$\left[\sigma_a^{\rm d}\right]^{(1)} \simeq \mathcal{B}\left\{\left[\ln\left(\frac{\beta^2}{1-\beta^2}\right)-\beta^2\right]S_0(a) + S_0(a)\ln(2m_{\rm e}c^2\,Q_1) - 2S_0(a)\,\ln[I_0(a)] + \int_{Q_1}^{Q_2}\frac{dQ}{Q}\,S_0(a;Q)\right\}, \tag{78}$$

where

$$S_0(a) = \int_0^\infty \frac{df_a(W)}{dW}\,dW \tag{79}$$

is the dipole sum, and

$$\ln[I_0(a)] = \frac{1}{S_0(a)}\int_0^\infty \ln W\,\frac{df_a(W)}{dW}\,dW. \tag{80}$$

The stopping cross section of the subshell is obtained by adding this result and the contribution of close interactions, Eq. (70) with the number $q_a$ of electrons in the subshell,

$$\left[\sigma_a^{\rm c}\right]^{(1)} \simeq \mathcal{B}\,q_a\left[\ln\left(\frac{2m_{\rm e}c^2\beta^2R}{(1-\beta^2)\,Q_2}\right)-\beta^2+\left(\frac{m_{\rm e}}{M}\beta^2\gamma R\right)^2\right]. \tag{81}$$

We thus find

$$\sigma_a^{(1)} = \mathcal{B}\left\{[S_0(a)+q_a]\left[\ln\left(\frac{\beta^2}{1-\beta^2}\right)-\beta^2\right] + 2\,S_0(a)\ln\left(\frac{2m_{\rm e}c^2}{I_0(a)}\right)+D_0(a) + q_a\left[\ln R+\left(\frac{m_{\rm e}}{M}\beta^2\gamma R\right)^2\right]\right\}, \tag{82}$$

with

$$D_0(a) = S_0(a)\ln\left(\frac{Q_1}{2m_{\rm e}c^2}\right) + \int_{Q_1}^{Q_2}\frac{dQ}{Q}\,S_0(a;Q) - q_a\ln\left(\frac{Q_2}{2m_{\rm e}c^2}\right). \tag{83}$$

#### 3. Energy-straggling cross section

The energy-straggling cross section for distant interactions with $Q < Q_2$ is [see Eq. (63)]

$$\left[\sigma_a^{\rm d}\right]^{(2)} \simeq \mathcal{B}\left\{\left[\ln\left(\frac{\beta^2}{1-\beta^2}\right)-\beta^2\right]S_1(a) + S_1(a)\ln\left(2m_{\rm e}c^2\,Q_1\right) - 2S_1(a)\,\ln[I_1(a)] + \int_{Q_1}^{Q_2}\frac{dQ}{Q}\,S_1(a;Q)\right\}, \tag{84}$$

with

$$S_1(a) = \int_0^\infty W\,\frac{df_a(W)}{dW}\,dW \tag{85}$$

and

$$\ln[I_1(a)] = \frac{1}{S_1(a)}\int_0^\infty W\,\ln W\,\frac{df_a(W)}{dW}\,dW. \tag{86}$$

The energy-straggling cross section of the subshell is obtained by adding to this result the contribution from close collisions, given by Eq. (71) with the number $q_a$ of electrons in the subshell. We thus obtain

$$\sigma_a^{(2)} = \mathcal{B}\left\{S_1(a)\left[\ln\left(\frac{\beta^2}{1-\beta^2}\right)-\beta^2\right] + 2S_1(a)\ln\left(\frac{2m_{\rm e}c^2}{I_1(a)}\right)+D_1(a) + q_a\left[(2-\beta^2)\,\frac{m_{\rm e}c^2\,\beta^2}{1-\beta^2}R+\frac{4}{3}\,\frac{m_{\rm e}^2}{M^2}\,\beta^6\gamma^4\,m_{\rm e}c^2R^3\right]\right\} \tag{87}$$

with

$$D_1(a) = S_1(a)\ln\left(\frac{Q_1}{2m_e c^2}\right) + \int_{Q_1}^{Q_2}\frac{dQ}{Q}\,S_1(a;Q) - q_a\,Q_2. \tag{88}$$

### D. Asymptotic formulas for atoms

The integrated cross sections for atoms are obtained by adding the contributions of the individual electron subshells with weights $q_a/(2|\kappa_a|)$.

#### *1. Total cross section*

The asymptotic formula for the total cross section is [see Eq. (76)]

$$\sigma^{(0)} = \sum_a \sigma_a^{(0)} = \mathcal{B}\left\{S_{-1}\left[\ln\left(\frac{\beta^2}{1-\beta^2}\right) - \beta^2\right] + 2\,S_{-1}\ln\left(\frac{2m_e c^2}{I_{-1}}\right) + D_{-1}\right\} \tag{89}$$

with

$$S_{-1} = \sum_a S_{-1}(a) = \int_0^\infty \frac{1}{W}\frac{df(W)}{dW}\,dW, \tag{90}$$

$$\ln[I_{-1}] = \frac{1}{S_{-1}}\sum_a S_{-1}(a)\,\ln[I_{-1}(a)] = \frac{1}{S_{-1}}\int_0^\infty \frac{1}{W}\,\ln W\,\frac{df(W)}{dW}\,dW, \tag{91}$$

and

$$D_{-1} = \sum_a D_{-1}(a). \tag{92}$$

Notice that the limits of the integral in the definition of $D_{-1}(a)$, Eq. (77), depend on the ionization energy $E_a$ of the subshell.

The expression (89) can be recast in a form similar to the conventional formula employed normally in the related literature,

$$\sigma^{(0)} = \mathcal{B}\left\{M_{\rm tot}^2\left[\ln\left(\frac{\beta^2}{1-\beta^2}\right) - \beta^2\right] + C_{\rm tot}\right\}, \tag{93}$$

where

$$M_{\rm tot}^2 = S_{-1} \tag{94}$$

is the total dipole-matrix element squared [3], and

$$C_{\rm tot} = 2\,S_{-1}\ln\left(\frac{2m_e c^2}{I_{-1}}\right) + D_{-1}. \tag{95}$$

We see that the total cross section $\sigma^{(0)}$ depends only on the speed and the charge of the projectile, but not on its mass. This feature is in contradistinction to the stopping and energy-straggling cross sections, which are different for particles with different masses and the same speed (see below). The parameters $M_{\rm tot}^2$ and $C_{\rm tot}$ are energy-independent constants, characteristic of the target atom or ion. The values of these parameters for free atoms, calculated from our numerical GOSs, are displayed in Fig. 4, which also shows the values obtained from non-relativistic calculations by Dehmer *et al.* [17] and Inokuti *et al.* [18] using the Hartree-Slater potential for the elements up to strontium ($Z \leqslant 38$). There is good agreement between the two calculations, because relativistic effects are small for these elements. It should be borne in mind that, because of the simplicity of our central-field approximation, the asymptotic formula with these constants may yield total cross sections that differ substantially from their actual values. Although total cross sections are very sensitive to aggregation effects, the formula (93), with appropriate values of the parameters $M_{\rm tot}^2$ and $C_{\rm tot}$, is valid also for inelastic collisions of charged projectiles with molecules or solids, (see, e.g., Ref. [19]).

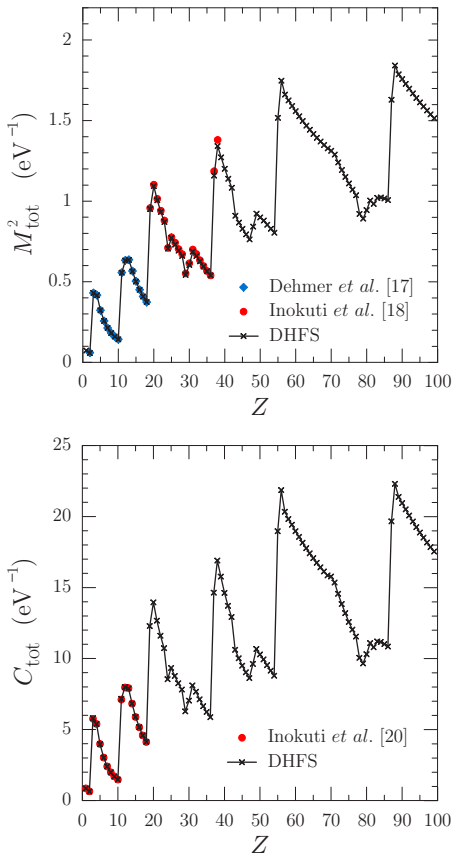


FIG. 4. Parameters of the asymptotic formula (93) of the total cross section for inelastic collisions with free neutral atoms, calculated from the present numerical GOS (crosses). The color circles are values from non-relativistic calculations in Refs. [17,18,20].

The formula (93) is analogous to the one derived by Fano [21], who considered only ionizing collisions and used the nonrelativistic GOS for longitudinal interactions and the dipole approximation for transverse interactions. Bethe [1] obtained the nonrelativistic analog of this formula for atomic hydrogen. As noted by Fano, a plot of the total cross section as a function of the quantity $\ln(\beta^2\gamma^2) - \beta^2$ is a straight line with slope $M_{\rm tot}^2$ and ordinate intercept $C_{\rm tot}$. This Fano plot has been used to assess the validity of the PWBA, and as a consistency check of experimental data (see, e.g., Refs. [3,22]).

### 2. Stopping cross section

The stopping cross section of the atom is obtained as [see Eq. (82)]

$$\sigma^{(1)} = \sum_a \sigma_a^{(1)} = \mathcal{B}\left\{[S_0 + Z]\left[\ln\left(\frac{\beta^2}{1-\beta^2}\right) - \beta^2\right] + 2\,S_0 \ln\left(\frac{2m_e c^2}{I_0}\right) + D_0 + Z\,f(\gamma)\right\} \tag{96}$$

with

$$S_0 = \sum_a S_0(a) = \int_0^\infty \frac{df(W)}{dW}\,dW, \tag{97}$$

$$\ln I_0 = \frac{1}{S_0}\sum_a S_0(a)\,\ln[I_0(a)] = \frac{1}{S_0}\int_0^\infty \ln W\,\frac{df(W)}{dW}\,dW, \tag{98}$$

$$D_0 = \sum_a D_0(a), \tag{99}$$

and

$$f(\gamma) = \ln(R) + \left(\frac{m_e}{M}\,\frac{\gamma^2-1}{\gamma}\,R\right)^2. \tag{100}$$

Figure 5 shows the dipole sum $S_0$ and the parameter $D_0$ calculated from the present numerical GOSs of neutral atoms.

It is interesting to compare the formula (96) with the conventional stopping power formula [23–25], which can be expressed as

$$\sigma^{(1)}_{\text{Bethe}} = \mathcal{B}\,2Z\left[\ln\left(\frac{2m_e v^2}{I}\right) + \ln\left(\frac{1}{1-\beta^2}\right) - \beta^2 + \frac{1}{2}\,f(\gamma)\right] \tag{101}$$

with the mean excitation energy $I$ defined by

$$\ln I = \frac{1}{Z}\int_0^\infty \ln W\,\frac{df(W)}{dW}\,dW. \tag{102}$$

The derivation of the Bethe formula (see, e.g., Ref. [5]) makes explicit use of the Bethe sum rule ($S_0(Q) = Z$), which is assumed to hold for any $Q$. Consequently, the formula is strictly valid only for light elements, for which relativistic deviations from the sum rule are small and do not modify appreciably the calculated stopping cross sections. In spite of this simplification, the Bethe formula (101) (with $Z$ interpreted as the number of electrons in a molecule and with a correction to account for the dielectric polarization of the medium) is considered to provide the molecular stopping cross section for arbitrary materials [10,24]. The only nontrivial parameter in the formula (101) is the mean excitation energy. Figure 6 displays the mean excitation energies of elemental materials recommended in the ICRU Report 37 [10], which were inferred from a combination of stopping power measurements and calculations for specific materials. Also shown are the values of the parameter $I_0$ calculated from the GOSs in our database.

The $I_0$ values and the ICRU empirical $I$ values are seen to vary similarly with $Z$, although the difference $I - I_0$ increases gradually with $Z$. The DHFS results are expected to be more accurate for the noble gas atoms than for other elements which naturally are in condensed phases or in molecular forms. The results in Fig. 6 show that our calculated $I_0$ values are close to the experimental values for He ($Z = 2$), Ne ($Z = 10$), and Ar ($Z = 18$), but are clearly too small for Kr ($Z = 36$), Xe ($Z = 54$), and Rn ($Z = 86$). The difference $I - I_0$ for high-$Z$ elements is partially due to the relativistic deviation from the Bethe sum rule.

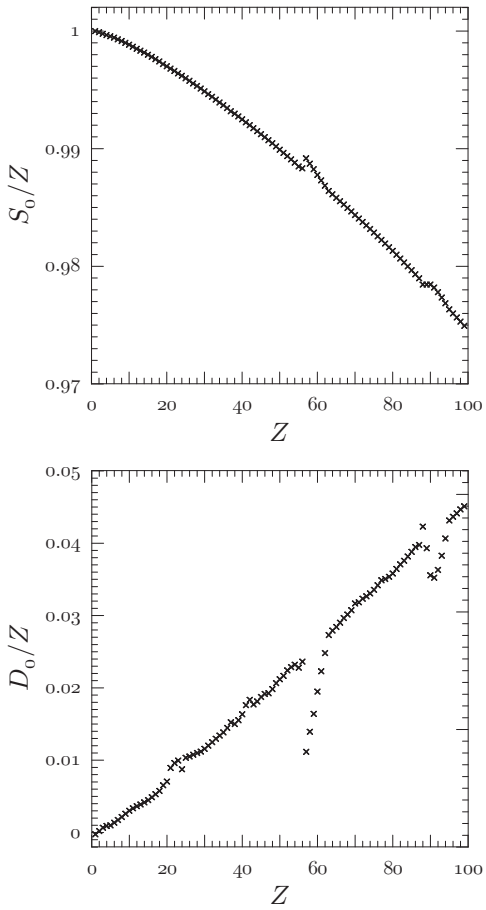


FIG. 5. Values of the dipole sum $S_0$ and the parameter $D_0$ calculated from the present database of numerical GOSs of neutral atoms. For the sake of clarity, the ratios $S_0/Z$ and $D_0/Z$ are plotted *versus* $Z$.

To verify the last assertion, we express the asymptotic formula (96) in a form as similar as possible to that of the Bethe formula (101). We write

$$\sigma^{(1)} = \mathcal{B}\,2Z\left\{\ln\left(\frac{2m_e v^2}{I_0'}\right) + \ln\left(\frac{1}{1-\beta^2}\right) - \beta^2 + \frac{1}{2}\,f(\gamma) + \frac{S_0 - Z}{2Z}\left[\ln\left(\frac{\beta^2}{1-\beta^2}\right) - \beta^2\right]\right\}, \tag{103}$$

where we have grouped the energy-independent terms by introducing the modified mean excitation energy $I_0'$ defined by

$$\ln\left(\frac{2m_e c^2}{I_0'}\right) = \frac{S_0}{Z}\,\ln\left(\frac{2m_e c^2}{I_0}\right) + \frac{D_0}{2Z}. \tag{104}$$

Evidently, Eq. (103) reduces to the Bethe formula when $S_0 = Z$ (the OOS satisfies the dipole sum rule) and $D_0 = 0$ (the Bethe sum rule is valid for all $Q$). Under these circumstances, we also have $I_0' = I_0 = I$.

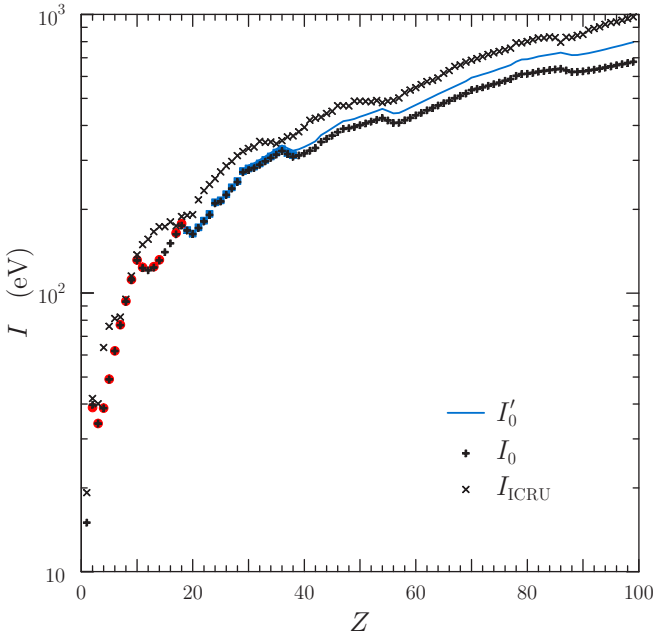


FIG. 6. Mean excitation energy of elemental substances versus the atomic number $Z$. The mean excitation energies recommended in the ICRU Report 37 [10] are represented by the times symbols. The red circles and blue squares are values calculated by Dehmer *et al.* [17] and by Inokuti *et al.* [18] with a nonrelativistic Hartree-Slater potential. Crosses indicate our calculated $I_0$ values, and the solid curve represents the modified mean excitation energies obtained from Eq. (104).

Figure 6 includes the values of $I_0'$ obtained from our DHFS calculations, which are seen to be closer to the empirical mean excitation energies. These results indicate that for the noble gases heavier than Ar nearly half the difference $I - I_0$ is due to the departure from the Bethe sum rule. We conclude that the usual definition of the mean excitation energy, Eq. (102), should be replaced with Eq. (104), which does account for that departure.

### 3. *Energy-straggling cross section*

The energy-straggling cross section for collisions of high-energy projectiles with atoms is given by [see Eq. (87)]

$$\sigma^{(2)} = \sum_a \sigma_a^{(2)} = \mathcal{B}\Big\{S_1\Big[\ln\Big(\frac{\beta^2}{1-\beta^2}\Big) - \beta^2\Big] + 2\,S_1 \ln\Big(\frac{2m_e c^2}{I_1}\Big) + D_1 + Z\,m_e c^2\,g(\gamma)\Big\}, \quad (105)$$

with

$$S_1 = \sum_a S_1(a) = \int_0^\infty W\,\frac{df(W)}{dW}\,dW, \quad (106)$$

$$\ln I_1 = \frac{1}{S_1}\sum_a S_1(a)\,\ln[I_1(a)] = \frac{1}{S_1}\int_0^\infty W\,\ln W\,\frac{df(W)}{dW}\,dW, \quad (107)$$

$$D_1 = \sum_a D_1(a), \quad (108)$$

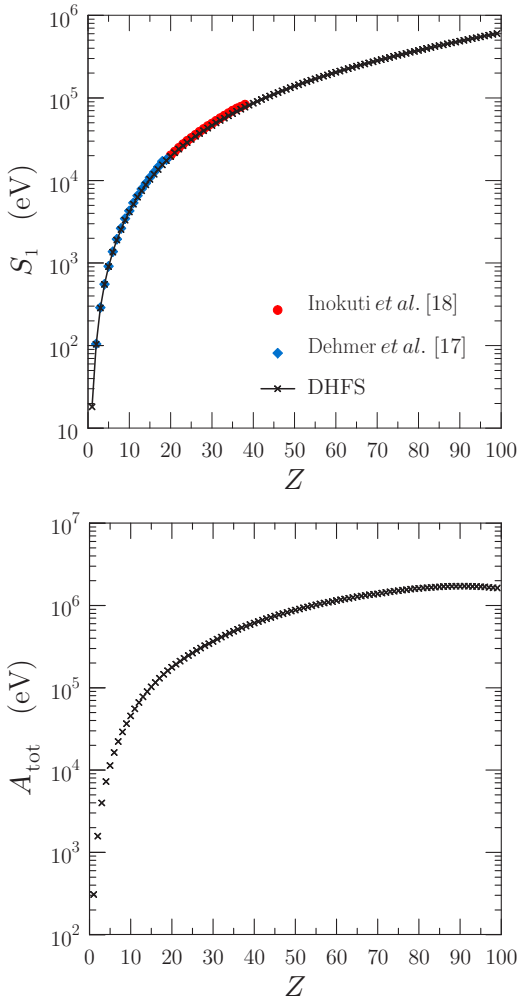


FIG. 7. Parameters $S_1$ and $A_{\rm tot}$ of the asymptotic formula (110) of the energy-straggling cross section for inelastic collisions with free neutral atoms, calculated from the present numerical GOS (crosses). The symbols are values obtained by Dehmer *et al.* [17] and Inokuti *et al.* [18] from nonrelativistic calculations.

and

$$g(\gamma) = \frac{\gamma^4 - 1}{\gamma^2}\,R + \frac{4}{3}\,\frac{m_e^2}{M^2}\,\frac{(\gamma^2-1)^3}{\gamma^2}\,R^3. \quad (109)$$

Grouping the energy-independent terms, we can write

$$\sigma^{(2)} = \mathcal{B}\Big\{S_1\Big[\ln\Big(\frac{\beta^2}{1-\beta^2}\Big) - \beta^2\Big] + A_{\rm tot} + Z\,m_e c^2\,g(\gamma)\Big\}, \quad (110)$$

where

$$A_{\rm tot} = 2\,S_1 \ln\Big(\frac{2m_e c^2}{I_1}\Big) + D_1. \quad (111)$$

The top plot of Fig. 7 shows the values of the parameter $S_1$ for free neutral atoms calculated from our numerical OOSs, together with values obtained by Dehmer *et al.* [17] and by Inokuti *et al.* [18] from nonrelativistic calculations with the Hartree-Slater potential for the elements with $Z = 1$–$38$. The

difference between these calculated values and ours increases gradually with the atomic number because of the increasing importance of relativistic effects. The bottom plot in Fig. 7 displays the calculated values of $A_{\rm tot}$. Because the parameters $S_1$ and $A_{\rm tot}$ depend strongly on the details of the excitation spectrum, our central-field approximation is not expected to give accurate values for materials other than the noble gases. Nonetheless, the asymptotic formula (110), with its parameters determined empirically for each material, is valid also for molecules and solids.

A classical formula for the energy-straggling cross section due to Bohr (Eq. (3.4.5) in Ref. [26]) is frequently referred to. Bohr's formula was derived by neglecting the binding of atomic electrons and using the nonrelativistic DCS for collisions with free electrons at rest. Later, Jackson [13] improved the formula by using the energy-loss DCS obtained from the relativistic PWBA [see Eqs. (66) and (67)],

$$\sigma^{(2)} \simeq \int_0^{W_{\rm ridge}} \mathcal{B}Z\left(1-\beta^2\frac{W}{W_{\rm ridge}}\right)dW.$$

This gives (Eq. (13.50) in Ref. [13])

$$\sigma^{(2)} = \mathcal{B}2Z\left[\gamma^2\beta^2 m_{\rm e}c^2\left(1-\frac{\beta^2}{2}\right)\right]. \qquad (112)$$

For comparison purposes, Fig. 10 below includes the energy-straggling cross sections of hellium, argon, and radon atoms calculated from this formula. The values obtained from expression (112) are nearly independent of $E$ at low energies, and a few percent larger than ours at energies higher than about 1 GeV, because of the neglect of electron binding effects.

## IV. NUMERICAL RESULTS FOR NOBLE GASES

The accuracy of the asymptotic formulas derived above can be assessed by direct comparison with integrated cross sections $\sigma^{(i)}$ obtained from the numerical integration of the DDCS times $W^i$. We present results for collisions with noble-gas atoms, for which the central-field approximation is expected to be more accurate than for atoms with open-shell configurations. Figures 8–10 display integrated cross sections for collisions of protons as functions of the kinetic energy of the projectile. We see that the differences between the numerical cross sections and the asymptotic formulas decrease smoothly when the energy of the projectile increases beyond a certain value, as expected for asymptotic formulas. For the total cross section, the differences become imperceptible, on the scale of the plots, for energies higher than about 1 MeV. Similarly, the curves of the asymptotic formulas and the numerical values of the stopping cross sections are seen to merge at energies of the order of 10 MeV. The asymptotic formula for the energy-straggling cross section agrees with the calculated values for energies larger than about 100 MeV. Of course, the asymptotic formulas (93), (103), and (110) should not be used for projectiles with lower energies.

It is worth observing that the larger the order $i$ of the integrated cross section $\sigma^{(i)}$ the higher the energy where the corresponding formula starts yielding reasonably accurate values, because of the increasing importance of large-$W$ interactions, part of which correspond to excitations of electrons in inner subshells. Therefore, the relative shell corrections (see the following section) are larger for the stopping cross section than for the total cross section, and even larger for the energy-straggling cross section.

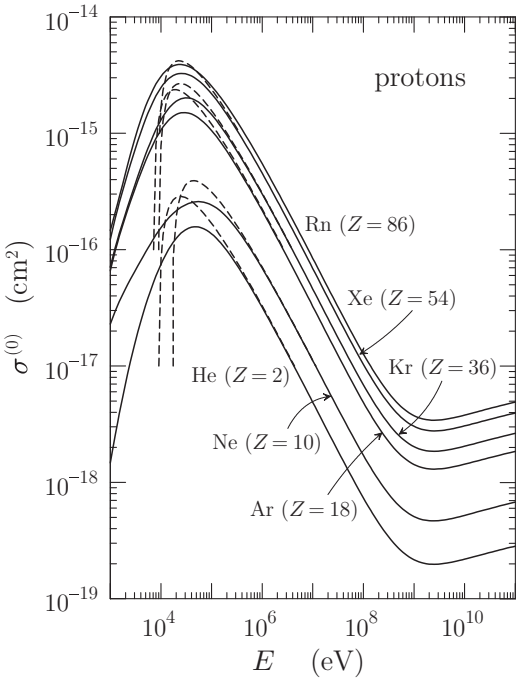


FIG. 8. Total cross sections, $\sigma^{(0)}$, for inelastic collisions of protons with noble-gas atoms as functions of the kinetic energy of the projectile. The solid curves represent results from numerical PWBA calculations. The dashed curves show the predictions of the asymptotic formula (93).

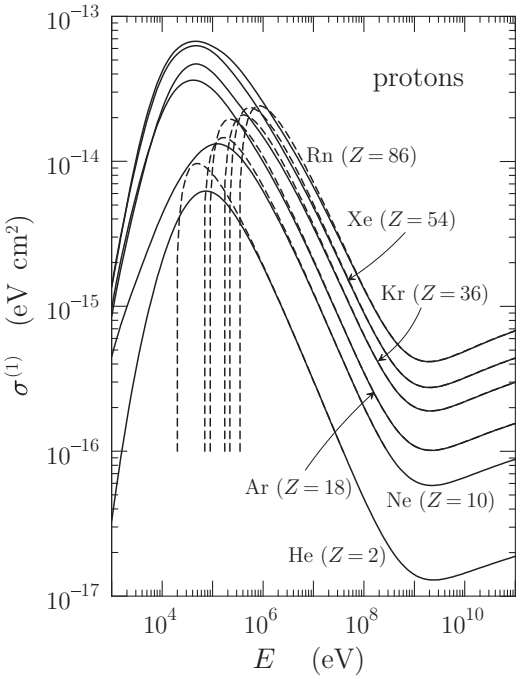


FIG. 9. Stopping cross sections, $\sigma^{(1)}$, for inelastic collisions of protons with noble-gas atoms. Dashed curves are predictions of the asymptotic formula (103). Other details as in Fig. 8.

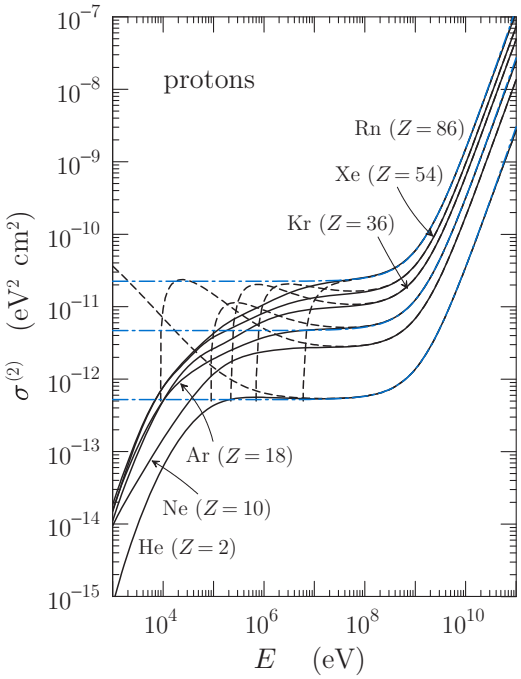


FIG. 10. Energy-straggling cross sections, $\sigma^{(2)}$, for inelastic collisions of protons with noble-gas atoms. Dashed curves are predictions of the asymptotic formula (110). The blue dot-dashed curves are the predictions of the formula (112) for He, Ar, and Rn. Other details as in Fig. 8.

The parameters of the asymptotic formulas were obtained by direct integration of the GOS by using numerical methods that are independent of those employed in the calculation of the integrated cross sections. The good agreement, at sufficiently high energies, between the numerical integrated cross sections and the asymptotic formulas indicates that the numerical algorithms used to interpolate and integrate the DDCSs remain accurate for energies up to $10^{11}$ eV. Nonetheless, for high-energy projectiles, the cross sections calculated numerically by integrating the DDCS are found to differ by up to 1% from the predictions of the asymptotic formulas. These differences arise from numerical errors accumulated during the calculations and, in the case of inner subshells with large ionization energies, from the approximations (48). For subshells with small and moderate ionization energies, say up to about 5 keV, and for high-energy projectiles, the difference between the subshell integrated cross sections obtained numerically and from the asymptotic formulas are typically less than about 0.5%.

## V. SHELL CORRECTIONS

The asymptotic formulas derived in the previous section result from some drastic approximations, whose accuracy deteriorates as the energy of the projectile decreases. The difference between the exact cross section $\sigma^{(i)}$ (i.e., the one obtained by integrating the DDCS) and the corresponding asymptotic formula is known as the shell correction. This name is motivated by the fact that the largest errors in the asymptotic formulas come from the contributions of the innermost subshells (i.e., those with the largest ionization energies). Since the wave functions of inner-shell electrons are quite insensitive to the effect of aggregation, shell corrections calculated for collisions with free atoms are expected to be approximately valid also for collisions in condensed media.

Previous theoretical calculations of shell corrections to the asymptotic formula for the stopping power were essentially nonrelativistic. Explicit formulas for the shell corrections in terms of the GOSs were obtained by subtracting from the integrals that define $\sigma^{(1)}$ those effectively used to calculate its asymptotic formula (see, e.g., Ref. [5]). Thus, Walske [27,28] used hydrogenic wave functions to obtain shell corrections for $K$ shell and $L$ subshells; Khandelwal and Merzbacher [29] and Bichsel [30] performed similar calculations for $M$ subshells. Bonderup [12] obtained an atomic subshell correction from stopping powers calculated using the local-plasma approximation of Lindhard and Scharff [31]. More recently, Bichsel [11] determined the corrections for the inner subshells of aluminum and silicon by direct integration of the nonrelativistic GOSs of Manson [32].

With our computational tools, the shell corrections can be obtained simply as the differences between the numerical integrated cross sections $\sigma^{(i)}_{\rm num}$ and the results from the asymptotic formulas. For this purpose, we define the shell corrections $\mathcal{C}^{(i)}$ so that the following formulas

$$\sigma^{(0)} = \mathcal{B}\left\{M_{\rm tot}^2\left[\ln\left(\frac{\beta^2}{1-\beta^2}\right) - \beta^2\right] + C_{\rm tot} - \mathcal{C}^{(0)}\right\}, \quad (113)$$

$$\sigma^{(1)} = \mathcal{B}\left\{2Z\left[\ln\left(\frac{2m_{\rm e}c^2}{I_0'}\right) + \ln\left(\frac{\beta^2}{1-\beta^2}\right) - \beta^2 + \frac{1}{2}f(\gamma)\right] + (S_0 - Z)\left[\ln\left(\frac{\beta^2}{1-\beta^2}\right) - \beta^2\right] - \mathcal{C}^{(1)}\right\}, \quad (114)$$

and

$$\sigma^{(2)} = \mathcal{B}\left\{S_{+1}\left[\ln\left(\frac{\beta^2}{1-\beta^2}\right) - \beta^2\right] + A_{\rm tot} + Z\,m_{\rm e}c^2\,g(\gamma) - \mathcal{C}^{(2)}\right\}, \quad (115)$$

reproduce the exact values of the integrated cross sections obtained by direct numerical integration of the DDCS. The expressions on the right-hand sides of these equations with $\mathcal{C}^{(i)} = 0$ are the asymptotic formulas for the atomic integrated cross sections $\sigma^{(i)}$. Evidently, each shell correction is proportional to the error of the associated asymptotic formula,

$$\mathcal{C}^{(i)} = \frac{1}{\mathcal{B}}\left(\sigma^{(i)}_{\rm asympt} - \sigma^{(i)}_{\rm num}\right). \quad (116)$$

Upon insertion of the calculated numerical cross section, this equation determines the correction $\mathcal{C}^{(i)}$.

The results displayed in Fig. 8 show that the shell correction $\mathcal{C}^{(0)}$ for protons with energies higher than about 1 MeV is small. At $E = 10$ MeV, the asymptotic formula (93) approximates the exact total cross to an accuracy better than about 0.1 percent. The shell correction $\mathcal{C}^{(2)}$ to the asymptotic formula of the energy-straggling cross section may be neglected for

proton energies higher than about $5Z$ MeV (see Fig. 10). At lower energies, the asymptotic formula departs rapidly from the exact cross section and it is preferable to use a tabulation of the numerical cross section $\sigma^{(2)}$ instead of the asymptotic formula.

The correction $\mathcal{C}^{(1)}$ to the stopping power formula is important because of the relevance of the stopping power in practical calculations of dosimetry and charged-particle transport. The asymptotic formula (103) for protons is found to differ from the numerical stopping cross section by less than about 1% for energies higher than about 100 MeV. At intermediate energies, say between 1 MeV and 100 MeV, the formula (103) yields values larger than the numerical ones. In the case of uranium ($Z = 92$), a maximum difference of about 7.5% is found at $E \sim 5$ MeV; for gold ($Z = 79$) the largest difference is 8.3% at $E \sim 4.5$ MeV. Because these differences are only one order of magnitude larger than the estimated numerical uncertainty of the calculated stopping cross sections, the resulting shell correction is very sensitive to accumulated numerical errors.

To conform with the literature, let us write the formula (114), as (cf. Refs. [5,23]),

$$\sigma^{(1)} = \mathcal{B}\,2Z\left\{\ln\left(\frac{2m_ec^2}{I_0'}\right) + \ln\left(\frac{\beta^2}{1-\beta^2}\right) - \beta^2 + \frac{1}{2}f(\gamma) - \frac{Z-S_0}{2Z}\left[\ln\left(\frac{\beta^2}{1-\beta^2}\right) - \beta^2\right] - \frac{C}{Z}\right\}, \tag{117}$$

where $C/Z = \mathcal{C}^{(1)}/2$ is the quantity usually referred to as the shell correction. The first term in the second line of this equation accounts for the departure from the dipole sum rule; it does not occur in the nonrelativistic theory.

Our calculated values of stopping cross sections for protons were used for determining the shell correction $C/Z$ to the stopping cross section. For low energies, up to $E_{\rm cut} = 0.2\,Z$ MeV, the correction was obtained by means of Eq. (116), that is, from the difference between the stopping cross section calculated numerically and the result of the asymptotic formula with $\mathcal{C}^{(1)} = 0$. Figure 11 displays the shell correction to the stopping cross section for collisions of protons with noble-gas atoms as functions of the kinetic energy of the projectile.

As mentioned above, the difference on the right-hand side of Eq. (116) magnifies the numerical errors accumulated throughout the calculation of the integrated cross section $\sigma^{(1)}_{\rm num}$. This is illustrated in Fig. 11 for the case of argon and kinetic energies higher than $E_{\rm cut}$, where the blue crosses represent the calculated numerical values. Although the magnitude of the errors in the calculated stopping cross sections is estimated to be less than about 0.5%, these errors blur the continuous curves of the shell correction as a function of the proton energy. To obtain a well-defined shell correction for energies higher than $E_{\rm cut}$, we approximate it in the form

$$\frac{C}{Z} = \sum_{n=1}^{6} c_n \left(\frac{m_{\rm p}c^2}{E}\right)^{n/4}, \tag{118}$$

where $m_{\rm p}$ is the proton mass. By similarity with the nonrelativistic theory, here we assume that the shell correction tends to zero at high energies. The parameters $c_n$ ($n = 1$–6) have been determined through a least-squares fit to the calculated stopping cross section $\sigma^{(1)}_{\rm num}$ for energies in the interval from

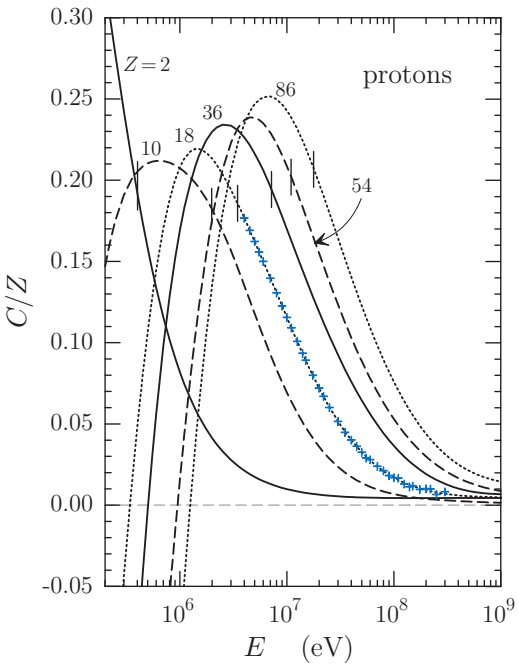


FIG. 11. Shell corrections $C/Z$ to the asymptotic formula of the stopping cross section for inelastic collisions of protons with noble-gas atoms, as functions of the kinetic energy of the projectile. The vertical segments indicate the energies $E_{\rm cut} = 0.2Z$ MeV above which the correction is described by the fitted formula (118). Crosses represent values obtained from Eq. (116), with visible fluctuations arising from numerical uncertainties of the calculated $\sigma^{(1)}_{\rm num}$ at energies higher than $\sim 10^8$ eV.

$E_{\rm cut}$ up to 1 GeV. In that energy interval, the analytical expression (118) with the fitted parameters approaches the calculated stopping cross sections with an accuracy generally better than 0.05% for all the elements. The fitted formula effectively averages the numerical errors and gives estimates of the shell correction that are probably better than the values obtained numerically from Eq. (116). Assuming that $C/Z$ remains constant for energies higher than 1 GeV, where the magnified numerical uncertainties do not allow determining the shell correction unambiguously, the relative difference between the Bethe formula and the calculated $\sigma^{(1)}_{\rm num}$ values remains less than 0.3% for energies up to 10 GeV. The fitting procedure provides evidence that numerical errors accumulated throughout the calculation of integrated cross sections are less than about 0.5% for energies up to 10 GeV.

It is important to notice that we are considering shell corrections that arise only from inaccuracies in approximating the integrated cross sections obtained from the PWBA. Chen *et al.* [33–35] went beyond the PWBA by using the perturbed-stationary-state approximation of Brandt and Lapicki [36], which accounts for (1) alterations in the binding of the active electron due to the presence of the projectile proton near the nucleus of the target atom, and (2) the deflection of the projectile path caused by the Coulomb field of the nucleus. Empirical shell corrections resulting from comparisons of the asymptotic formulas with these more elaborate calculations, and with experimental data, would account also for the simplifications implicit in the PWBA.

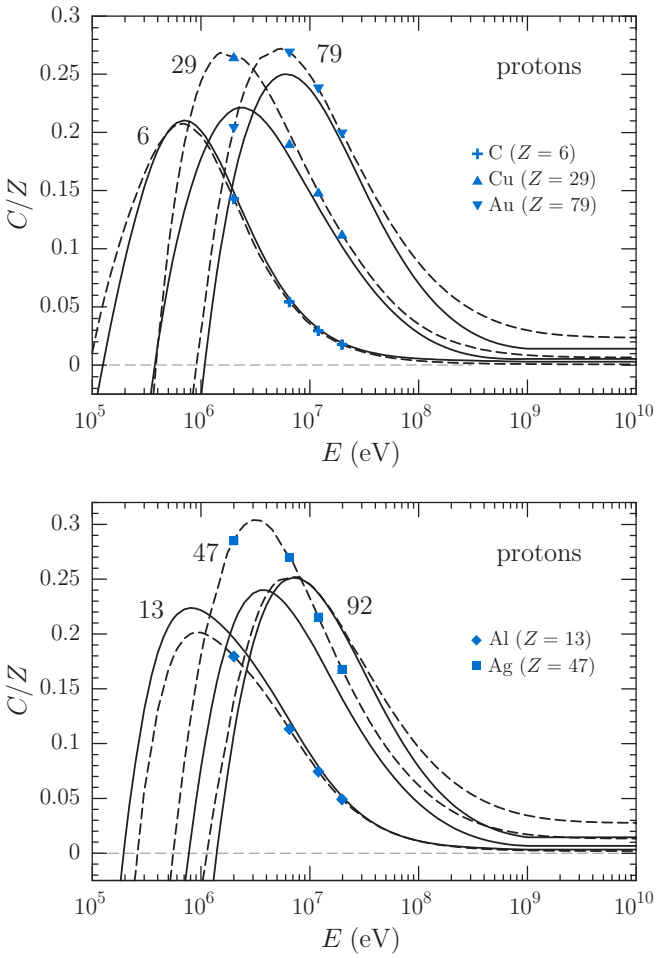


FIG. 12. Shell corrections $C/Z$ to the asymptotic formula of the stopping cross section for inelastic collisions of protons with atoms of the elements with the indicated atomic numbers, as functions of the kinetic energy of the projectile. Solid curves are the present results, symbols are Bichsel's semiempirical shell corrections given in the ICRU Report 37 [10], and the dashed curves were generated with the program BEST of Berger and Bichsel [37].

Figure 12 displays the shell correction to the stopping cross sections for collisions of protons with atoms of the elements C ($Z = 6$), Al ($Z = 13$), Cu ($Z = 29$), Ag ($Z = 47$), Au ($Z = 79$), and U ($Z = 92$), as functions of the kinetic energy of the projectile. Also shown are the values of Bichsel's (Model 1) semiempirical shell correction given in the ICRU Report 37 [10] and calculated with the program BEST [37]. It is worth noticing that Bichsel [24] derived the shell correction and the mean excitation energy $I$ from a multiparametric fit to available experimental stopping-power data for the elements C, Al, Cu, Ag, and Au of the formula [cf. Eq. (101)]

$$\sigma_{\rm Bethe}^{(1)} = \mathcal{B}\,2Z\Bigg[\ln\left(\frac{2m_{\rm e}v^2}{I}\right) + \ln\left(\frac{1}{1-\beta^2}\right) - \beta^2 + \frac{1}{2}f(\gamma) - \frac{C}{Z} - \frac{\delta}{2} + L_1(\beta) + L_2(\beta)\Bigg], \quad (119)$$

where $\delta/2$, $L_1(\beta)$, and $L_2(\beta)$ are, respectively, the density-effect correction, the Barkas correction, and the Bloch correction [24]. At intermediate energies near the maximum of the $C/Z$ curves, our calculated corrections agree reasonably with Bichsel's estimates for C and U, are sensibly larger for Al, and smaller for Cu, Ag, and Au. The differences between our shell corrections and Bichsel's estimates are much larger than the numerical inaccuracies of our calculated data. These differences are caused by the neglect of the relativistic departure from the Bethe sum rule, which is implicit in Eq. (119), and by the consideration of the density effect, Barkas, and Bloch corrections in Bichsel's fit.

## VI. CONCLUDING REMARKS

The relativistic PWBA, combined with the independent-electron DHFS model, allows the calculation of accurate longitudinal and transverse GOSs. We have computed a numerical database of GOSs for all subshells of neutral atoms from hydrogen ($Z = 1$) to einsteinium ($Z = 99$) in their ground-state configurations. This database exhibits the known relativistic departure from the Bethe sum rule. We have derived asymptotic formulas of the total cross section, the stopping cross section, and the energy-straggling cross section for collisions of charged particles heavier than the electron with neutral atoms. Calculations for protons have shown that these asymptotic formulas are consistent with cross sections calculated numerically by integrating the energy-loss DCS. The asymptotic formula for the stopping cross section [Eq. (103)] has the same form as the conventional Bethe formula [Eq. (101)], except for the fact that the mean excitation energy $I$ [Eq. (102)] is to be replaced with the modified value defined by Eqs. (104) and (98), and a small additional term [second line of Eq. (103)] is to be added. A central result of our study is that the definition of the mean excitation energy should be modified for high-$Z$ elements to account for the departure from the Bethe sum rule.

The calculated total, stopping, and energy-straggling cross sections allow the systematic calculation of shell corrections from the differences between the numerical values and the prediction of the corresponding asymptotic formulas. In the case of the stopping cross section, this approach is free from interference with effects beyond the PWBA (such as the Barkas and Bloch corrections [24]). The resulting shell correction is expected to be more reliable than current estimates and models. It can be used, e.g., for determining the modified mean excitation energy $I_0'$ from available experimental data by following a procedure similar to the one described by Ziegler [25].

The parameters in the asymptotic formulas calculated from the present approach are found to be consistent with nonrelativistic results from the literature. A numerical tabulation of the parameters displayed in the plots, for the elements with $Z = 1$–99, is available from the authors and will be published elsewhere together with tables of the calculated shell correction to the stopping cross section.

## ACKNOWLEDGMENTS

Financial support from the Spanish Ministerio de Ciencia, Innovación y Universidades/Agencia Estatal de Investigación/European Regional Development Fund, European Union, (Project No. RTI2018-098117-B-C22) is gratefully acknowledged.

[1] H. A. Bethe, Zur Theorie des Durchgangs schneller Korpuskularstrahlen durch Materie, Ann. Phys. **397**, 325 (1930).

[2] H. A. Bethe, Bremsformel für Elektronen relativistischer Geschwindigkeit, Z. Phys. **76**, 293 (1932).

[3] M. Inokuti, Inelastic collisions of fast charged particles with atoms and molecules — The Bethe theory revisited, Rev. Mod. Phys. **43**, 297 (1971).

[4] M. Inokuti, Y. Itikawa, and J. E. Turner, Adenda: Inelastic collisions of fast charged particles with atoms and molecules — The Bethe theory revisited, Rev. Mod. Phys. **50**, 23 (1978).

[5] U. Fano, Penetration of protons, alpha particles and mesons, Annu. Rev. Nucl. Sci. **13**, 1 (1963).

[6] D. Bote and F. Salvat, Calculations of inner-shell ionization by electron impact with the distorted-wave and plane-wave Born approximations, Phys. Rev. A **77**, 042701 (2008).

[7] F. Salvat and J. M. Fernández-Varea, RADIAL: a Fortran subroutine package for the solution of the radial Schrödinger and Dirac wave equations, Comput. Phys. Commun. **240**, 165 (2019), see also the manual of the computer code.

[8] S. M. Cohen, Bethe stopping power theory for heavy-element targets and relativistic projectiles, Phys. Rev. A **68**, 012720 (2003).

[9] S. M. Cohen, Range of validity for perturbative treatments of relativistic sum rules, Phys. Rev. A **68**, 042704 (2003).

[10] ICRU Report 37, *Stopping Powers for Electrons and Positrons* (ICRU, Bethesda, 1984).

[11] H. Bichsel, Shell corrections in stopping powers, Phys. Rev. A **65**, 052709 (2002).

[12] E. Bonderup, Stopping of swift protons evaluated from statistical atomic model, Mat. Fys. Medd. Dan. Vid. Selsk. **35**, 1 (1967).

[13] J. D. Jackson, *Classical Electrodynamics*, 2nd ed. (John Wiley and Sons, New York, 1975).

[14] M. E. Rose, *Relativistic Electron Theory* (John Wiley and Sons, New York, 1961).

[15] J. S. Levinger, M. L. Rustgi, and K. Okamoto, Relativistic corrections to the dipole sum rule, Phys. Rev. **106**, 1191 (1957).

[16] F. Salvat, PENELOPE-*2018: A code System for Monte Carlo Simulation of Electron and Photon Transport*, OECD Nuclear Energy Agency, document NEA/MBDAV/R(2019)1, Boulogne-Billancourt, France, 2019, https://doi.org/10.1787/32da5043-en.

[17] J. L. Dehmer, M. Inokuti, and R. P. Saxon, Systematics of moments of dipole oscillator-strength distributions for atoms of the first and second row, Phys. Rev. A **12**, 102 (1975).

[18] M. Inokuti, J. L. Dehmer, T. Baer, and J. D. Hanson, Oscillator-strength moments, stopping powers, and total inelastic-scattering cross sections of all atoms through strontium, Phys. Rev. A **23**, 95 (1981).

[19] J. M. Fernández-Varea, R. Mayol, D. Liljequist, and F. Salvat, Inelastic scattering of electrons in solids from a generalized oscillator strength model using optical and photoelectric data, J. Phys.: Condens. Matter **5**, 3593 (1993).

[20] M. Inokuti, R. P. Saxon, and J. L. Dehmer, Total cross-sections for inelastic scattering of charged particles by atoms and molecules – VIII. Systematics for atoms in the first and second row, Int. J. Radiat. Phys. Chem. **7**, 109 (1975).

[21] U. Fano, Ionizing collisions of very fast particles and the dipole strength of optical transitions, Phys. Rev. **95**, 1198 (1954).

[22] C. J. Powell, X. Llovet, and F. Salvat, Use of the Bethe equation for inner-shell ionization by electron impact, J. Appl. Phys. **119**, 184904 (2016).

[23] S. P. Ahlen, Theoretical and experimental aspects of the energy loss of relativistic heavily ionizing particles, Rev. Mod. Phys. **52**, 121 (1980).

[24] ICRU Report 49, *Stopping Powers and Ranges for Protons and Alpha Particles* (ICRU, Bethesda, 1993).

[25] J. F. Ziegler, The stopping of energetic light ions in elemental matter, J. Appl. Phys. / Rev. Appl. Phys. **85**, 1249 (1999).

[26] N. Bohr, The penetration of atomic particles through matter, K. Dan. Vidensk. Selsk. Mat. Fys. Medd. **18**, 1 (1948).

[27] M. C. Walske, The stopping power of K-electrons, Phys. Rev. **88**, 1283 (1952).

[28] M. C. Walske, Stopping power of L-electrons, Phys. Rev. **101**, 940 (1956).

[29] G. S. Khandelwal and E. Merzbacher, Stopping power of M electrons, Phys. Rev. **144**, 349 (1966).

[30] H. Bichsel, Stopping power of M-shell electrons for heavy charged particles, Phys. Rev. A **28**, 1147 (1983).

[31] J. Lindhard and M. Scharff, Energy loss in matter by charged particles of low charge, Dan. Mat. Fys. Medd. **27**, 1 (1953).

[32] S. T. Manson, Inelastic collisions of fast charged particles with atoms: ionization of the aluminum L shell, Phys. Rev. A **6**, 1013 (1972).

[33] M. H. Chen, B. Crasemann, and H. Märk, Relativistic calculation of atomic M-shell ionization by protons, Phys. Rev. A **27**, 2358 (1983).

[34] M. H. Chen and B. Crasemann, Relativistic cross sections for atomic K- and L-shell ionization by protons, calculated from a Dirac-Hartree-Slater model, At. Data Nucl. Data Tables **33**, 217 (1985).

[35] M. H. Chen and B. Crasemann, Atomic K, L-, and M-shell cross sections for ionization by protons: a relativistic Hartree-Slater calculation, At. Data Nucl. Data Tables **41**, 257 (1989).

[36] W. Brandt and G. Lapicki, L-shell Coulomb ionization by heavy charged particles, Phys. Rev. A **20**, 465 (1979).

[37] M. J. Berger and H. Bichsel, BEST, BEthe STopping power program (unpublished). (This program was used to generate the high-energy stopping power tables given in the ICRU report 49, Ref. [24]).